Zn-Phthalocyanine / C$_{60}$

Solar Cells

Diplomarbeit zur Erlangung des akademischen Grades

Diplom Ingenieur

im Diplomstudium

Wirtschaftsingenieurwesen - Technische Chemie

angefertigt am

Linz Institute for Organic Solar Cells (LIOS)

eingereicht von

Martin Egginger

unter der Betreuung von

o. Univ. Prof. Dr. Serdar N. Sariciftci

Co-Betreuung:

Ass. Prof. Dr. Helmut Neugebauer

Prof. Dr. Dr.h.c. Dieter Meissner

Linz, April 2005

dedicated to

July and Laura

ZUSAMMENFASSUNG

Organische Zweischicht Solarzellen mit Zink-Phthalocyanin als p-artiger und Fulleren C_{60} als n-artiger Halbleiter werden untersucht.

AFM Messungen zeigen Cluster auf der Oberfläche der organischen Filme. Die Größe dieser Cluster und damit die Filmrauhigkeit hängen von der Aufdampfrate ab. Photolumineszenz Messungen legen nahe, dass nur ein dünner Bereich am Interface zum Photostrom beiträgt. Dennoch haben Solarzellen mit 50 nm ZnPc und 75 nm C_{60} die höchsten Effizienzen. Strom-Spannungs Messungen zeigen, dass unter Belichtung starke Photoleitung (sekundärer Photostrom) berücksichtigt werden muss und dass viele Solarzellen Gegendioden haben.

Spannungsabhängige Photostrom Messungen zeigen eine Wurzelabhängigkeit des Photostrom Signals, welches dem primären Photostrom zugeordnet werden kann, mit angelegter Spannung. Das stimmt mit dem Gärtner Modell überein und unterstützt die Existenz einer Raumladungszone am Interface.

ABSTRACT

Organic bilayer heterojunction solar cells using zinc - phthalocyanine as p-type and fullerene C_{60} as n-type material were investigated.

AFM measurements show clusters at the surface of the organic layers. The cluster size and therefore the film roughness of the organic layers depend on the growth rate. Photoluminescence measurements indicate that only a small region around the interface contributes to the photocurrent. Nevertheless the devices with 50 nm ZnPc and 75 nm C_{60} have the highest efficiencies. Current-voltage measurements reflect that under illumination strong photoconductivity (secondary photocurrent) has to be taken into account and many devices show back diodes.

Voltage dependent photocurrent measurements show a square root dependence of the photocurrent signal which can be attributed to the primary photocurrent with applied voltage. This agrees with the Gärtner model and supports the existence of a space-charge-region at the interface.

TABLE OF CONTENTS

ACKNOWLEDGEMENT

1 INTRODUCTION

1.1. World Energy Demand and Solar Cells

The world energy demand is steadily increasing. Fossil fuels and nuclear energy are at the moment the main energy sources for the world. All these resources are limited. The peak of depletion of mineral oil might be as soon as 2006 [1]. A big problem is that the CO_2 emissions of burned fossil fuels cause global warming. Uranium does not cause CO_2 emissions but has always been under intensive public discussions because of the imminent danger of nuclear power stations and the following problems with the radioactive waste.

All these problems would be solved by using renewable energies. Solar energy is an unlimited energy source that can be used all over the world. The European Union plans to increase the contribution of renewable energies from 14 to 23.5 % until the year 2015. By then photovoltaics installed capacity shall be increased by a factor of 100 [2].

At the moment the main part of installed photovoltaic modules are silicon based. However production of crystalline silicon solar cells is extremely energy and therefore cost intensive. One way to reduce the costs are organic thin film solar cells. Organic dyes fulfil many requirements to be used in solar cells: They have high absorption coefficients and many of them show p- or n-type semiconductor behaviour. Various cheap coating technologies are available: spin coating, doctor blading, thermal evaporation, ink jet printing, etc. Organic solar cells are light weight and have high environmental sustainability. Another advantage is the possibility to change the colour of an organic solar cell for architectural purposes [3].

Until now there are no organic solar cells on the market. However Siemens announced to be able to produce organic solar cells with 5 % efficiency by printing on flexible substrates [4].

1.2.   Aim of this thesis

Since Tang reported on organic solar cells using copper-phthalocyanine and a perylene derivative reaching 1 % efficiency [5] enormous efforts have been made to improve organic solar cells. One type of organic solar cells are those prepared from small molecules: In this thesis solar cells consisting of zinc-phthalocyanine (ZnPc) and Buckminster fullerene (C_{60}) are investigated. In previous investigations very often CuPc and ZnPc have been used. Efficiencies obtained for CuPc and ZnPc are higher than those using other central atoms in the phthalocyanine. ZnPc was chosen as p-type material here. In previous investigations [6, 7, 8] MPP [9] and ZnPc were used. Because of recently reported [10] high efficiencies using C_{60} as electron acceptor n-type material it was used in this work.

The main goal of this work was to build ZnPc / C_{60} heterojunction bilayer devices and characterize them. A special goal was the investigation of the voltage dependence of the photocurrent spectra to evaluate whether a basic model used for silicon solar cells is also applicable for organic bilayer heterojunction solar cells and to get a closer insight into the working principle of these solar cells.

Another part was the setup of a high vacuum evaporation system in which co-evaporation from two temperature- and four current-controlled boats is possible. The system (Leybold Univex 350) is already installed and running at the institute but the experimental part of this work was finished before finishing the installation. Therefore details of the new system are not described in this work.

The following sub-sections of chapter 1 will explain the theory of organic solar cells needed for the discussion of this work. In chapter 2, device preparation, the materials and measurement setups used in these studies are explained. Chapter 3 contains the results of these investigations. In chapter 4 these results will be discussed considering theoretical models described in chapter 1. The work finishes with a short conclusion.

1.3. ZnPc / C_{60} Solar Cells

A lot of work has been done since Tang introduced the first organic solar cell [5]. Here just some important studies on Pc / C_{60} solar cells will be listed. For detailed information the reader is referred to review articles [e.g. 11, 12].

Recently, the investigation of devices consisting of multiple coevaporated layers with varying CuPc - C_{60} – ratio: ITO / 3.5 nm CuPc / 16 nm CuPc:C_{60} (3:1) / 16 nm CuPc:C_{60} (1:1) / 16 nm CuPc:C_{60} (1:3) / 5 nm C_{60} / 12 nm BCP [13] / 100 nm Al showed efficiencies of 1.36 % [14]. However the devices containing mixed layers show much faster degradation than the pure heterojunctions.

Another report was on p-i-n solar cells: ITO / PEDOT:PSS / 50 nm p-m-MTDATA [15] / 50 nm ZnPc:C_{60} (1:2) / 50 nm n-MPP [16] / 1 nm LiF / 70nm Al were investigated [17]: The calculated efficiencies are 3.37 % at 10 mW / cm² and 1.04 % at 100 mW / cm² under white light illumination from a xenon lamp.

Introducing an additional organic layer (called "exciton blocking layer") to the device ITO / PEDOT:PSS / 5 nm CuPc / 20 nm C_{60} / 10 nm BCP / 80 nm Al is reported to result in efficiencies of 3.6 % under 1.5 suns [18]. Tandem cells with CuPc / CuPc:C_{60} (1:1) / C_{60} as active layers for both cells are reported recently to show efficiencies up to 5.7 % [10].

A strong influence of oxygen on ZnPc devices was observed [19]. This influence was not further investigated during this work. For ZnPc devices it was shown [20] that O_2 influences the rectification ratio: No rectification is observed in Au / ZnPc / Metal devices unless the device is exposed to air. Rostalski [6] showed that a way to eliminate back diodes (the diode starts to open in forward direction, but then the current increases slower again) in MPP / ZnPc devices is exposing the device to air for several days.

Day and Price showed that the conductivity increases when exposing ZnPc to air [21].

Investigating p-n sandwich cells: ITO / 78 – 240 nm MPP / 164 – 300 nm ZnPc / 50 nm Au, Günster et al. [22] concluded that the charge carrier generation only occurs in small regions at the p / n – or Schottky – type contacts. However, they assume that the photoconductivity is a true bulk effect. These two effects have different recombination processes leading to different intensity dependences.

The thickness of the active (space charge) region in a Mpp / ZnPc heterojunction device is calculated to be 5 nm in ZnPc [23].

A problem that is often observed when two materials are mixed ("bulk" phase) is phase separation. One possibility to avoid this phase separation is to covalently bind them together. Ab initio calculations for ZnPc-C_{60} supramolecules were performed and predicted good efficiencies for devices made with these molecules [24]. Investigating devices consisting of a MDMO-PPV:PCBM mixture with added ZnPc-C_{60} showed an increase in the photocurrent in the range of 700 nm (ZnPc absorption) compared to cells without the ZnPc-C_{60} molecule, but low short-circuit currents indicate charge transport problems [25, 26].

1.4. Theory

1.4.1. Workfunctions

The nature of a contact between a semiconductor and a metal or between two semiconductors is determined by the workfunctions: the energetic differences between the Fermi levels and the vacuum levels. The relative values determine whether the contact is either an ohmic or a Schottky contact (see 1.4.2).

Figure 1 shows the different workfunctions (E_F) for ITO, PEDOT:PSS and Al together with the conduction band (E_c) and valence band (E_v) level of ZnPc and HOMO (highest occupied molecular orbital) and LUMO (lowest unoccupied molecular orbital) of C_{60}. For the influence of LiF on the Al contact see 2.1.3. The workfunction of ITO heavily depends on the preparation technique and various surface treatments, therefore a maximum and a minimum value found in literature are shown.
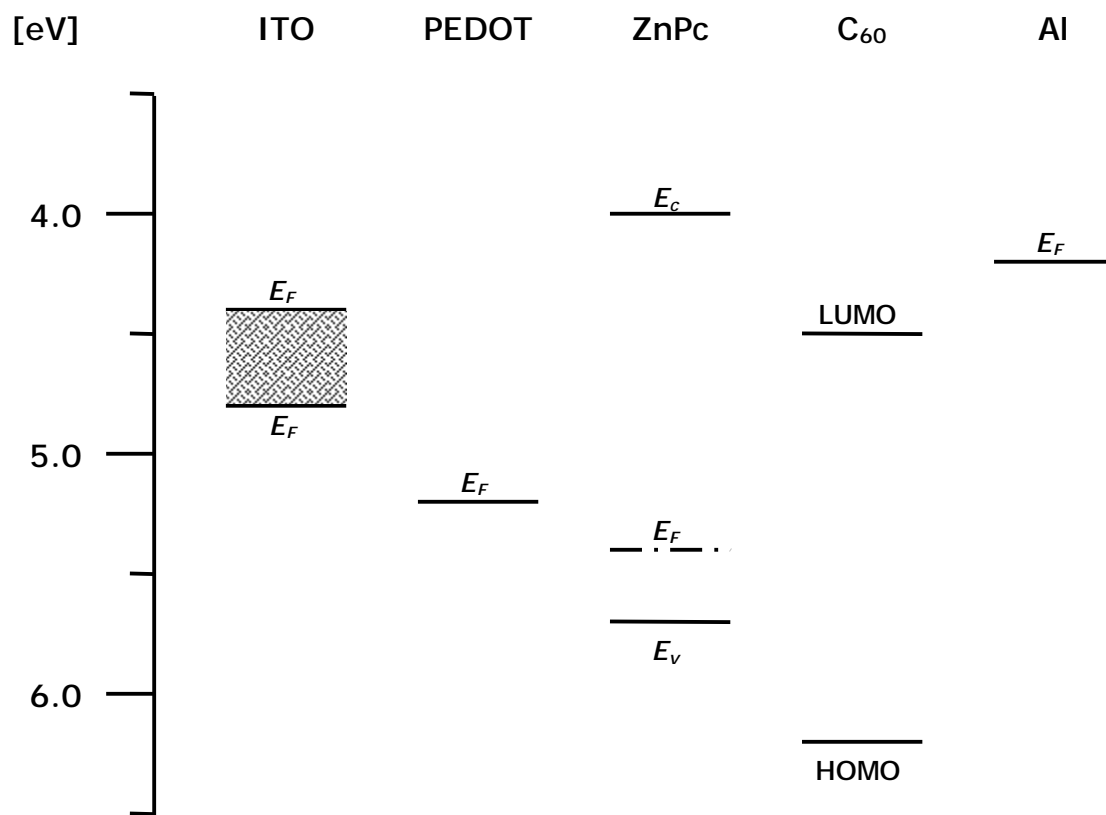
Figure 1: Workfunctions versus vacuum of ITO [27, 28, 29], PEDOT [27] and Al [30], E_c, E_v and E_{Fermi} of ZnPc [31] and HOMO and LUMO of C_{60} [32, 33].

1.4.2. Semiconductor / Metal - Contacts

If the workfunction of the n-type semiconductor Φ_s is smaller than the workfunction of the metal Φ_M a rectifying (Schottky) contact is formed. The barrier height $q\Phi_b$ is $q\Phi_M - X_s$, where X_s is the electron affinity of the semiconductor. The band bending $q\Phi_D$ and therefore the maximum achievable photovoltage of this kind of contact is $q(\Phi_M - \Phi_s)$.
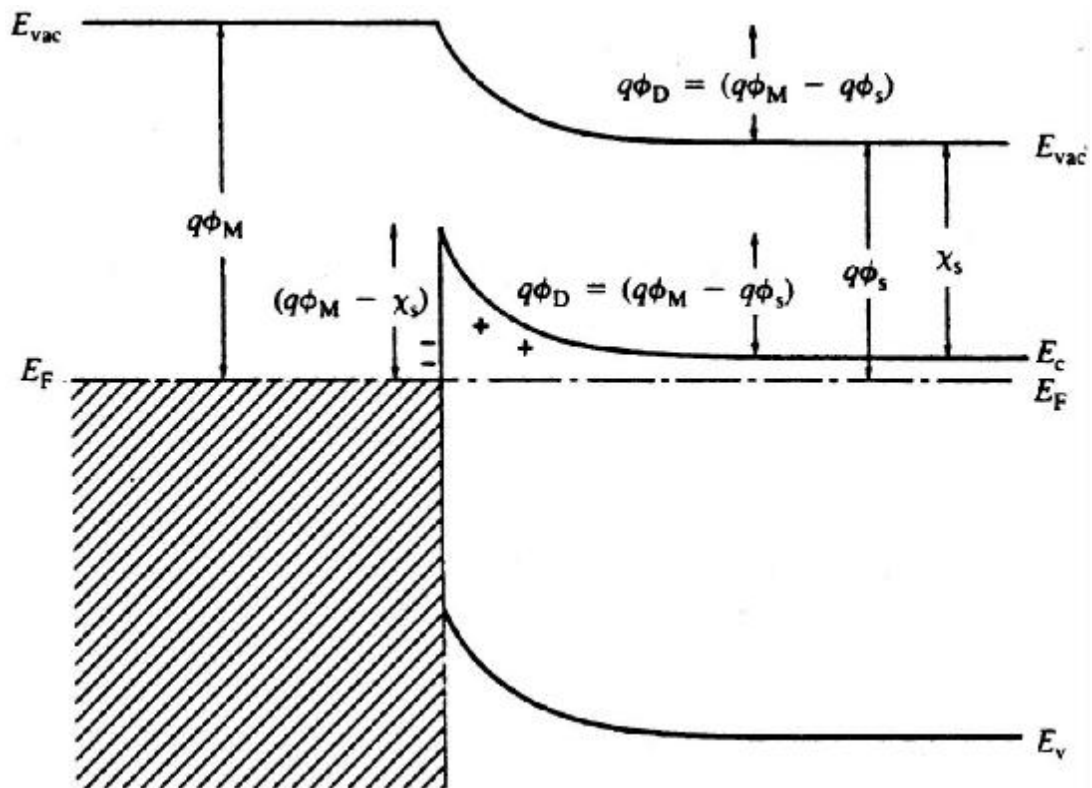
Figure 2: Rectifying (Schottky) contact of a metal and a n-type semiconductor (taken from [34]).

If the workfunction of the n-type semiconductor Φ_s is larger than the workfunction of the metal Φ_M an ohmic contact is formed. This is shown in Figure 3:
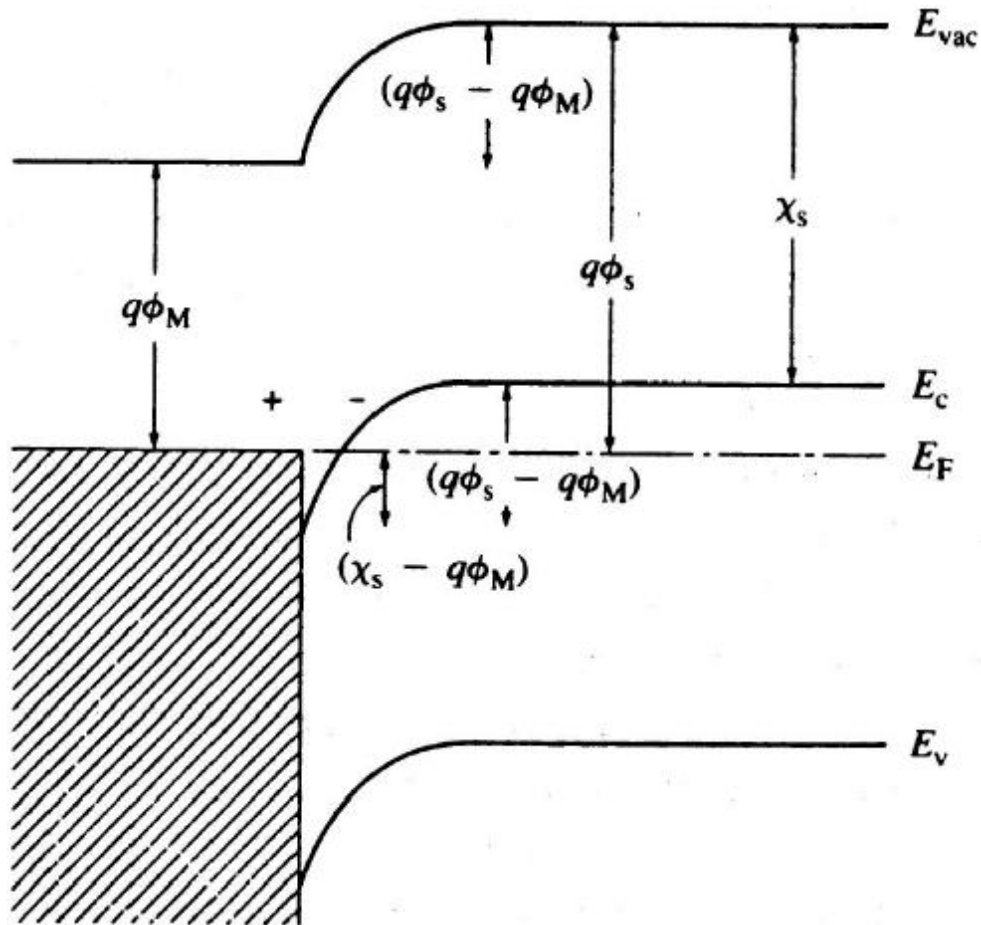
Figure 3: Ohmic contact of a metal and a n-type semiconductor (taken from [34]).

1.4.3. p / n – Contacts

A contact of a p-doped material and the same material n-doped is called a homo p / n - contact. If the p-type and the n-type material are different materials, the contact is called a hetero p / n – contact.

1.4.3.1. Homo p / n - Contact

If a p-type and a n-type semiconductor of the same material form a contact, the fermi levels approach each other by charge diffusion. Electrons of donor atoms of the n-type material flow to acceptor atoms of the p-type material. Charges on doping atoms, which are fixed next to the contact, form a space-charge region and lead to band bending at the contact.
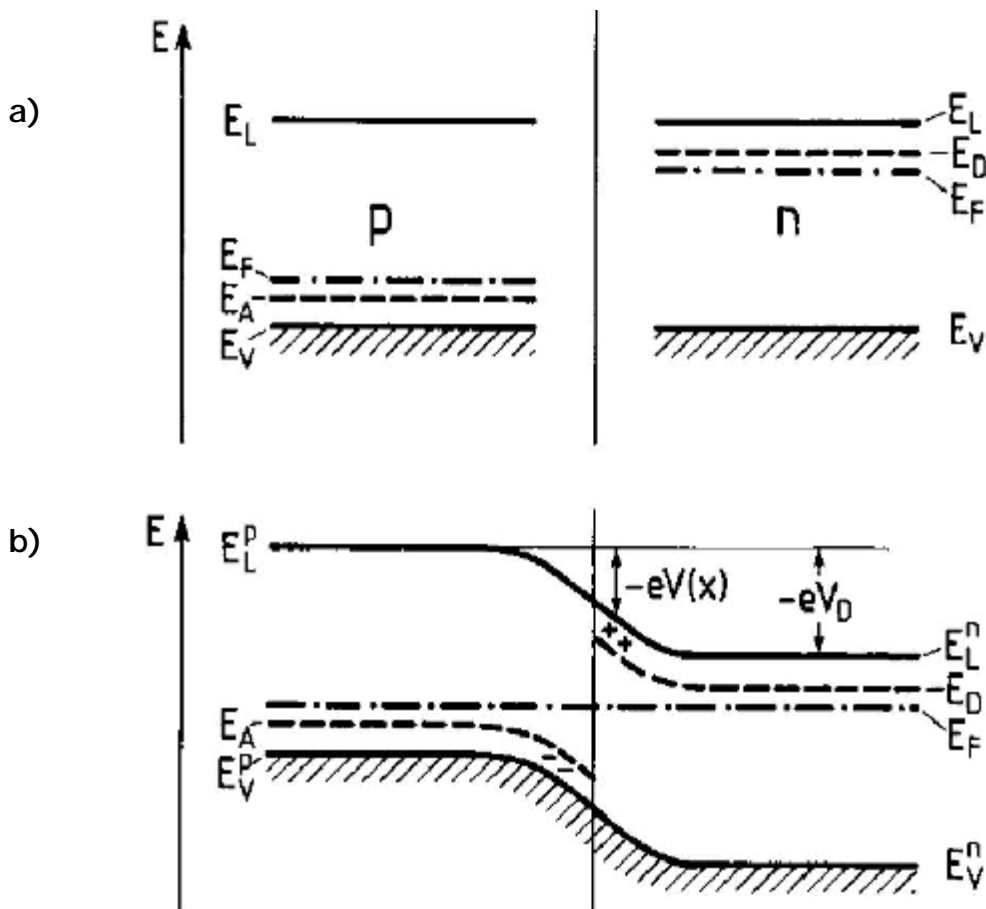
Figure 4: Band scheme of a p-type (left) and a n-type (right) semiconductor before (a) and after (b) contact (taken from [35]).

Figure 4 shows a homo p / n contact: the conduction band (E_L), the valence band (E_v), the Fermi level (E_F), the acceptor states (E_A) and the donor states (E_D) are shown.

1.4.3.2. Hetero p / n - Contact

ZnPc and C_{60} have different material parameters: band gap (E_g), electron affinity (A_c), ionization energy (I_c) and different workfunctions (Φ) lead to different bands. Figure 5 shows the energy scheme of two different materials before contact:
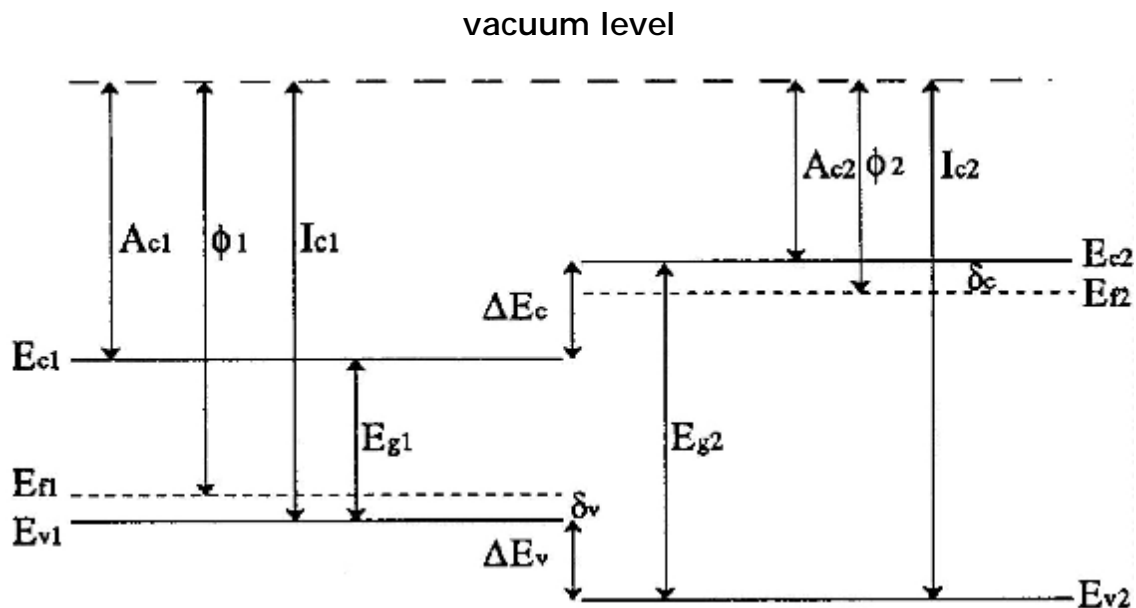
Figure 5: Energy scheme of two different semiconductors before contact (taken from [8]).

Figure 6 shows the energy scheme of the materials shown in Figure 5 after contact: The Fermi energies align, but due to the different band edges (ΔE_c and ΔE_v shown in Figure 5) there are discontinuities in the conduction and in the valence band.
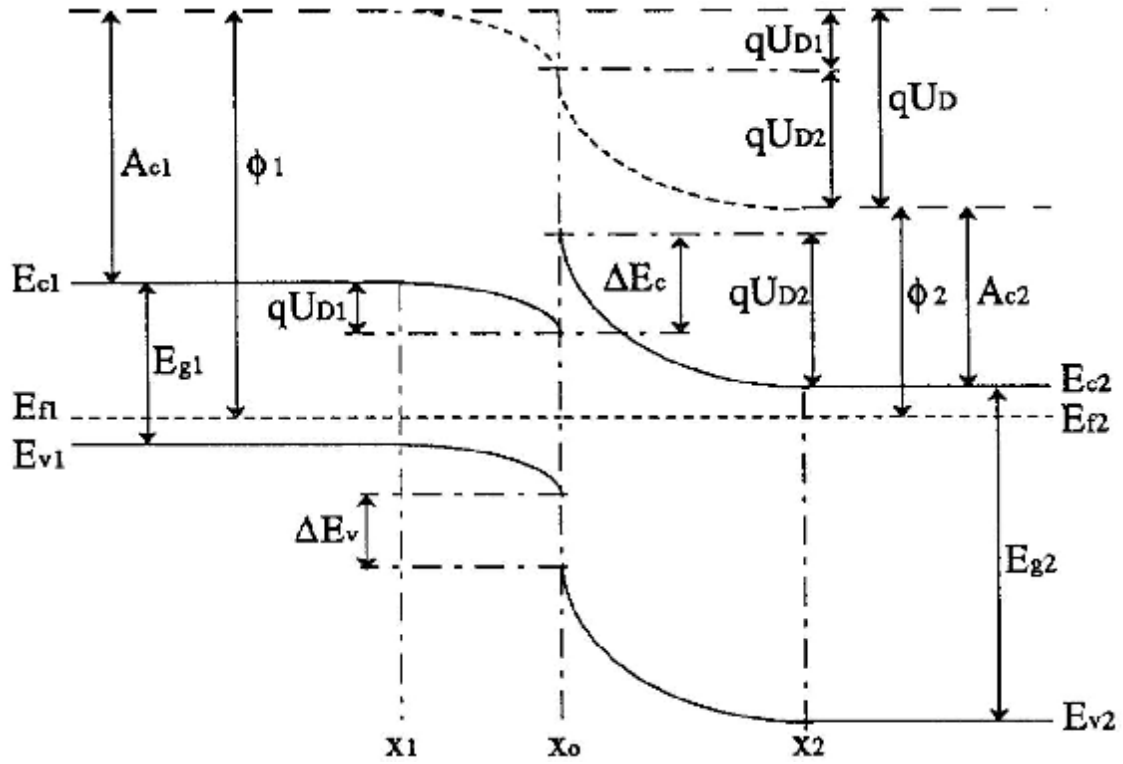
Figure 6: Band scheme of a hetero p / n – contact (taken from [8]).

1.4.3.3. Current – Voltage characteristic and Space Charge Region

For an ideal p / n junction the Shockley equation [36] describes the current (*J*) – voltage (*V*) characteristic:

$$j = j_p + j_n = j_0 \left(e^{\frac{qU}{kT}} - 1 \right)$$ **Equation 1**

with

$$j_0 = \frac{q D_p p_{n_0}}{L_p} + \frac{q D_n n_{p_0}}{L_n}$$ **Equation 2**

In these equations j_n and j_p are the electron and the hole current density, respectively. D_n and D_p are the diffusion constants, L_n and L_p are the diffusion lengths, U is the applied voltage and j_0 is the saturation current

14

density, which is defined by material parameters [6]. j_0 includes the minority charge carrier concentrations p_{n_0} and n_{p_0}. Under illumination the generated photocurrent j_{ph} has to be added to the Shockley equation (Equation 1).

The Gärtner model [37] describes j_{ph} (Equation 3) for an illuminated p / n contact. Here **I** is the photon flux, **a** is the absorption coefficient, **W** is the thickness of the space charge region and L_p is the minority charge carrier diffusion length:

$$j_{ph} = -eI_0\left(1 - \frac{e^{-aW}}{1 + aL_p}\right)$$

Equation 3

For the case $L_p << W << a^{-1}$ this equation can be simplified to:

$$j_{ph} = -eI_0aW = const.*W$$

Equation 4

The thickness of the space charge region of a p / n junction is proportional to the square root of the total contact potential difference:

$$W = \left(const.*V_K\right)^{1/2}$$

Equation 5

Equation 4 and Equation 5 add up to:

$$j_{ph} = const.\left(V - V_{fb}\right)^{1/2}$$

Equation 6

where V_{fb} is the flat band potential. A less restrictive necessity allowing also for minority carriers non negligible diffusion lengths is $W << a^{-1}$. For this case Equation 3 can be simplified to:

$$j_{ph} = const.\left(L_p + W\right)$$

Equation 7

Therefore, if the Gärtner model is applicable for organic bilayer heterojunction solar cells, it is expected that j_{ph} is proportional to the square root of the applied voltage.

1.4.4. Excitons

Another approach to describe the basic mechanism of charge carrier generation is via excitons [11, 12]:

The absorbed photon leads to an excited state, the exciton. In this exciton the hole and the electron are bound to each other, therefore they can be described as one non-charged particle. This exciton can diffuse. Pettersson et al. give a number for the average exciton diffusion length in C_{60}: 7.7 nm [38]. If the exciton reaches a hetero-contact, the electron and the hole are separated immediately. Afterwards charges may reach the electrodes. If the electric field of a space charge region is high enough (e.g. larger than 10^5 V / cm), excitons might also be split here.

Under the assumption of charge carrier generation only at the interface and highly efficient extraction of the generated charge carriers an external field should not influence the photocurrent.

2 EXPERIMENTAL

2.1.   Device Preparation

Solar Cells of the structure shown in Figure 7 were built:
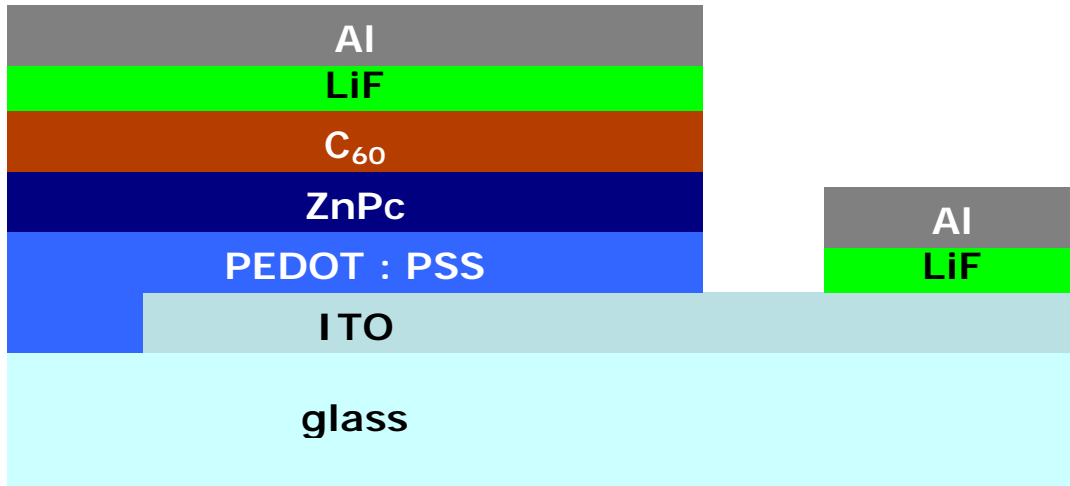
Figure 7: Scheme of a solar cell: ITO covered glass / spin-cast PEDOT:PSS / evaporated ZnPc / evaporated C_{60} / evaporated top electrodes (LiF / Al)

2.1.1. Substrate Preparation

Indium-tin-oxide (ITO) coated glass sheets (purchased from Merck KGaA, Darmstadt, Germany, with an ITO thickness of d = 125 nm and a sheet resistance < 15 $\Omega \square$) were cut into 1.5 * 1.5 cm² substrates. To prevent short circuits when contacting the top electrodes, some part of the ITO was removed by etching: A strong acid ($HCl_{conc.}$: $HNO_{3 \ conc.}$: H_2O = 4.6 : 0.4 : 5) was applied to 1/3 of the ITO - surface. The rest of the surface was covered with a nail polish as protection against the acid. After 20 min the acid was washed away with deionized water. Then the nail polish was removed with acetone. The etched substrates were cleaned

twice with acetone in an ultrasonic bath and finally with isopropanole in an ultrasonic bath, each for 15 min.

Glass substrates for UV-Vis absorption and AFM measurements were also cleaned in ultrasonic baths as described above.

2.1.2. Organic Materials

2.1.2.1. PEDOT:PSS

Before evaporation of the active layer an electrochemically oxidized mixture of poly(3,4-ethylenedioxythiophene) and poly(styrenesulfonate) (PEDOT:PSS) (purchased from Bayer AG, Leverkusen, Germany) was spin coated twice onto the ITO. (Aqueous dispersion with particle size of 80 nm and 0.5 w% PEDOT:PSS = 2:3.) Before spin coating the PEDOT:PSS dispersion was stirred for 10 min and afterwards filtered with a 0.45 µm filter. The following spin coating program was used: The samples were accelerated during a 4 s ramp to 1500 rpm and kept at that speed for 40 s. Afterwards they were accelerated to 2000 rpm and kept at that speed for 20 s. The coated devices were dried under vacuum for at least 60 min and afterwards stored under Ar over night.

PEDOT:PSS is used as an interfacial hole conducting and electron blocking layer. Figure 8 shows the chemical structure:
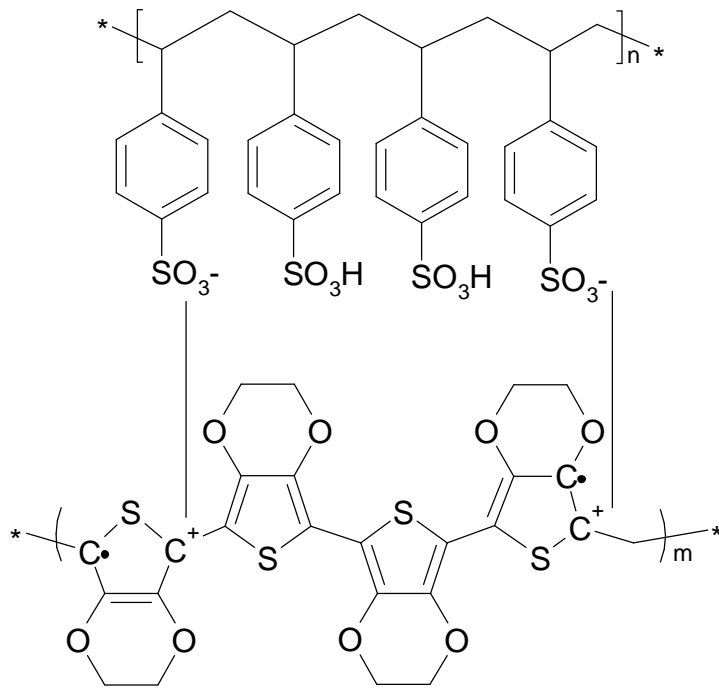
Figure 8: 2-dimensional chemical structure of electrochemically doped poly(3,4-ethylenedioxythiophene) and poly(styrenesulfonate), PEDOT:PSS.

2.1.2.2. Zink-Phthalocyanine

The organic dye zinc-phthalocyanine (ZnPc), purchased from Fluka Chemie AG, Buchs, Switzerland, was used for charge generation and as a hole conducting p-type material. ZnPc was sublimed twice for purification and stored in air. ZnPc was evaporated (as well as C_{60}) under high vacuum (better than $5 * 10^{-6}$ torr) in an Edwards evaporation chamber (Edwards High Vacuum E12E3, BOC Edwards, Butzbach, Germany). The evaporation rate was monitored by a quartz balance, Intellemetrics IL 820 (Intellemetrics Ltd., Glasgow, UK). If not stated otherwise the growth rate for ZnPc and C_{60} were in a range of 0.2 to 0.3 nm / s.

There are 4 alumina crucibles in the evaporation chamber. ZnPc and C_{60} were evaporated one after the other without breaking the vacuum in between.

Figure 9 shows the chemical structure of ZnPc:
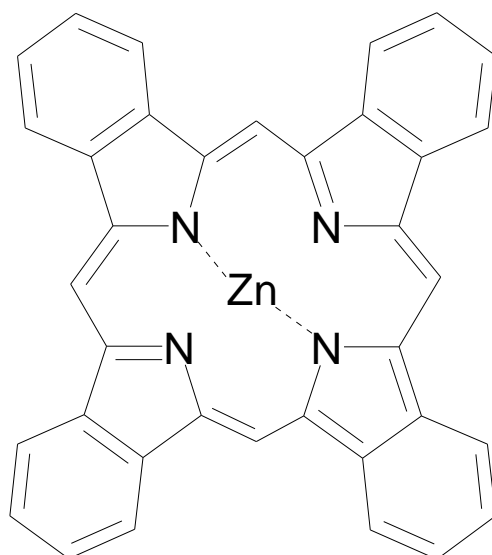
Figure 9: Chemical structure of zn-phthalocyanine (ZnPc).

2.1.2.3. Buckminsterfullerene (C_{60})

Buckminsterfullerene (here called C_{60}) was used as n-type semiconducting charge generating material. First time identified in 1985 [39] it attracted great interests among scientists.

During this work C_{60}, most probably bought at MER Corporation (Arizona, USA) was used without further purification (pureness 99.9 %). C_{60} was stored in an Ar – glovebox and only the small amount needed for evaporation was transferred (through air) into the evaporation system. For details concerning evaporation of C_{60} see section 2.1.2.2. Figure 10 shows the chemical structure of C_{60}:

Figure 10: Chemical structure of Buckminsterfullerene (C_{60}).

2.1.3. Top Contacts Evaporation

After evaporation of the active materials (ZnPc and C_{60}) the devices were transferred into an Ar-glovebox (M. Braun, Garching, Germany). During the transfer the devices were exposed to air. Further processing and measurements were performed in Ar gloveboxes:

0.6 nm of LiF and at least 80 nm of Al (to ensure good contact and good light reflection) were thermally evaporated under high vacuum

(around 1 * 10^{-5} mbar) in a Leybold evaporation chamber (Leybold Vacuum, Cologne, Germany). Tungsten boats were used. The evaporation rate (0.005 nm / s for LiF and 0.01 increasing to 0.3 nm / s for Al) was monitored by a quartz balance, Intellemetrics IC 600. In order to define the device area, the evaporation was done through a shadow mask.

Thin interfacial layers of LiF are known to improve the electron extraction, respectively the injection [40]. An increase in fill factors and stabilization of high V_{oc}'s are observed [41].

2.2.   AFM Measurements

Atomic force microscope (AFM) measurements were done with a Dimension 3100″ instrument from Digital Instruments (Santa Barbara, CA) in the tapping mode.

For thickness measurements films on glass substrates were mechanically scratched and afterwards the stepheight was measured.

2.3.   UV-Vis Absorption Spectroscopy

The UV-Vis measurements were performed using a HP 8453 spectrometer (Hewlett-Packard, Palo Alto, CA, USA). To determine the optical constants needed for thickness measurements a Carry 3 G spectrometer (Varian, Palo Alto, CA, USA) was used.

2.4.   Photoluminescence Measurements

The photoluminescence (PL) was measured in reflection geometry using a home-made setup (for detailed setup information see [42]). The samples were in a cryostat and evacuated to approximately 1E-5 mbar. The homemade cold finger cryostat can be cooled with liquid nitrogen. The samples were excited by a chopped (mechanical chopper, SR 540, Stanford Research Systems, Sunnyvale, CA, USA) laser beam (l = 664 nm), from a diode laser (Aerotech, Pittsburgh, USA) with 45 mW (before the chopper wheel) on a beam spot of an area of 10 mm². The PL signal was focused on the entrance of the monochromator (Polytec, Waldbronn, Germany) and was detected (Si detector: Polytec, Waldbronn, Germany, for wavelengths < 1100 nm) after amplification using a lock-in amplifier, Stanford Model SR 830.

2.5.   Current - Voltage Measurements

The measurements were carried out in Ar-gloveboxes. The Steuernagel solar simulator (K. H. Steuernagel Lichttechnik GmbH, Mörfelden-Walldorf, Germany, with a metal halogen lamp as light source and with an AM 1.5 filter) was calibrated to 100 mW/cm². The J - V curves were measured with a Keithley 2400 (Keithley Instruments, Inc., Cleveland, Ohio, USA) sweeping from -2 V to +2 V. ITO was used as the positive electrode, Al as the negative electrode.

A J - V measurement gives the important parameters to describe a solar cell: The open-circuit voltage (V_{oc}), the short-circuit current (J_{sc}) and the maximum-power-point (*mpp*) defined as the point inside the fourth quadrant (power-quadrant) where the product of J times V has a maximum. The mpp defines the maximum-power voltage (V_{mpp}) and the maximum-power current (J_{mpp}). In Figure 11 these 4 parameters are explained:
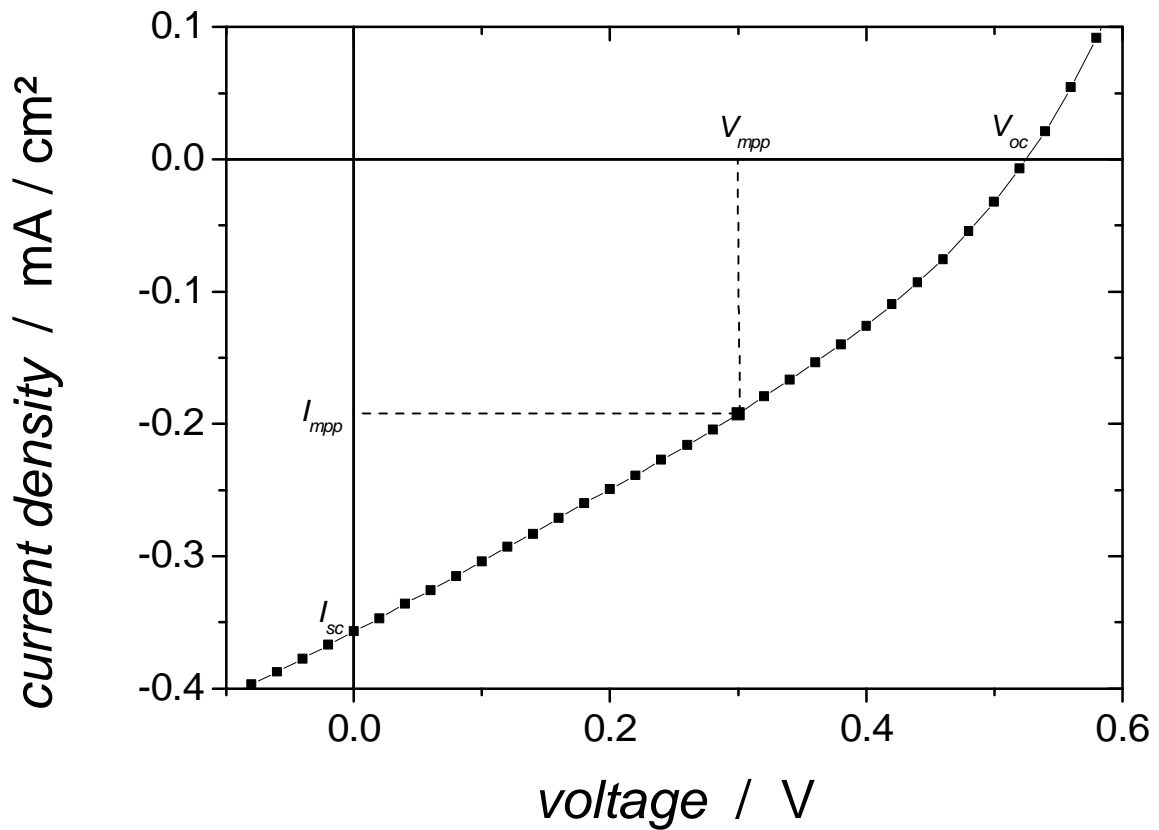
Figure 11: Definition of V_{oc}, J_{sc}, V_{mpp} and J_{mpp}.

From these parameters other parameters can be calculated: The fill factor (*FF*) describes the quality of the diode in the power quadrant:

$$FF = \frac{V_{mpp} * J_{mpp}}{V_{oc} * J_{sc}}$$
  Equation 8

For ideal diodes the *FF* approaches 1. With the *FF* the efficiency can be calculated. (See Lewerenz [37] for definition of AM 1.5.)

$$\eta_{AM1.5} = \frac{I_{sc} * V_{oc} * FF}{P_{light}}$$
  Equation 9

2.6.   *IPCE* Measurements

The incident-photon-to-current-efficiency (*IPCE*), also referred to as incident-photon-to-collected-electron-efficiency, gives the spectral resolution of the photocurrent.

These measurements were done in Ar-gloveboxes using a home made setup: The light coming from a 80 W Xe-lamp (Müller Elektronik Optik LXH100, Moosinning, Germany) is optically chopped (Scitec Instruments Ltd. 300C, Cornwall, UK) with 73 Hz. After passing a monochromator (Acton Research Corp. FA448M, Acton, MA, USA) the light is focused onto the sample using a light fibre. Each time the lamp is turned on, the lamp spectrum is calibrated using a monocrystalline silicon diode with known sensitivity (Melles Griot, Carlsbad, CA, USA). For signal detection a lock-in amplifier (EG&G Instruments 7260, Gaithersburg, MD, USA) is used. After the measurement the *IPCE* can be calculated:

$$IPCE \ [\%] = 1240 \ [\text{V*nm}] \ * \ \frac{I \ [\text{nA}]}{\lambda \ [\text{nm}] * Ip \ [\text{nW}]} \ * \ 100 \qquad \textbf{Equation 10}$$

In this equation I_p is the light power incident on the device.

For voltage dependent *IPCE* measurements a power supply was put in series to the lock-in and to the device. During the first measurements a homemade voltage-supply unit (using the local electricity supply; power up to 2.5 V) was used. The later measurements were done using a 1.5 V battery as power supply and a potentiometer to tune the voltage. The battery was used up to 1000 mV.

The absolute current values in an *IPCE* measurement are in the range of some nA. Investigating changes of these small intensities caused by an applied external voltage (see 3.5.2) raises the question how constant the measurement system is. Therefore, frequency dependence of the signal and stability of the Xe-lamp over time have been investigated:
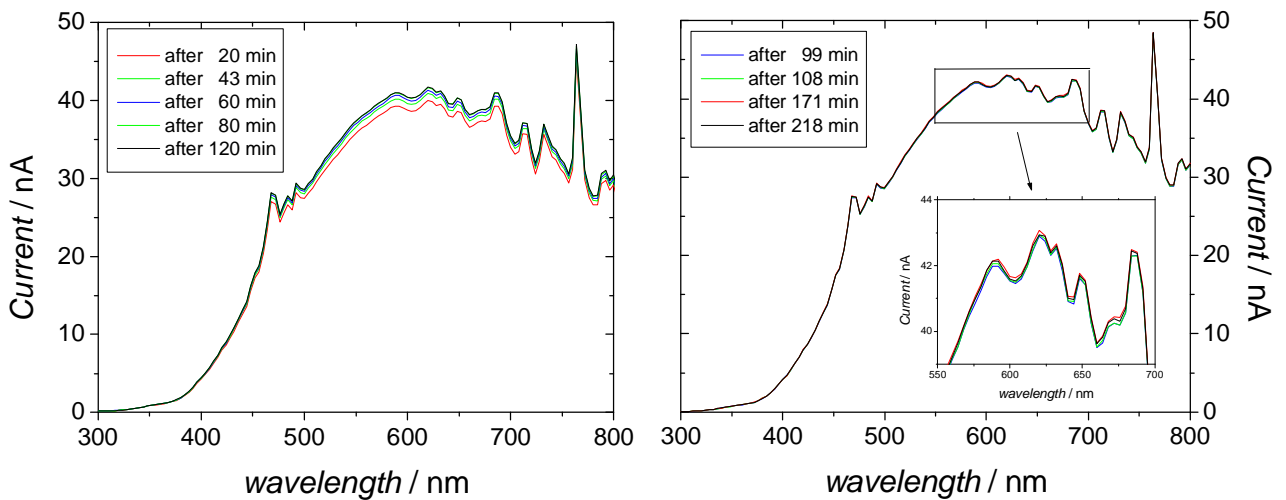
Figure 12: Stability of the Xe-lamp. Left: within 120 min after turning on the lamp. Right: 99 to 218 min after turning on.
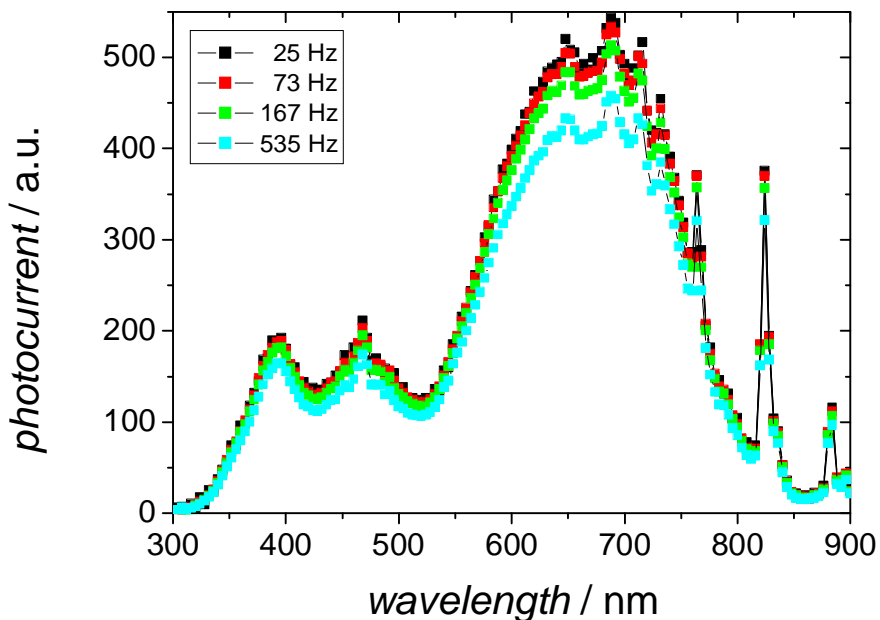
Figure 13: Frequency dependence of the *IPCE* signal.

It is shown that the lamp reaches a stable intensity after 60 min (Figure 12) and that the signal is not frequency dependent (Figure 13) for the low frequency of 73 Hz used here. For higher frequencies the signal decreases: obviously the device cannot follow the intensity change any more.

3 RESULTS

3.1. AFM Measurements

AFM measurements were applied to check the roughness of the films. This is important for the modelling of the investigated thin film solar cells: Does a material make a real film (which would mean that the whole device is covered with the material) or are there just islands of the material spread within the device?

The second reason to be interested in the film roughness is optical modelling (section 4.4): *IPCE* measurements are compared to an optical model. A required simplification of the model is that the interfaces between the layers are completely flat.

3.1.1. Substrates and PEDOT:PSS

AFM pictures and corresponding cross-sections of a glass substrate after cleaning, an ITO substrate after cleaning and a PEDOT:PSS film spin-cast onto a clean ITO substrate are given here. Figure 14 (A) shows the glass substrate, (B) the ITO substrate and (C) the PEDOT:PSS film.
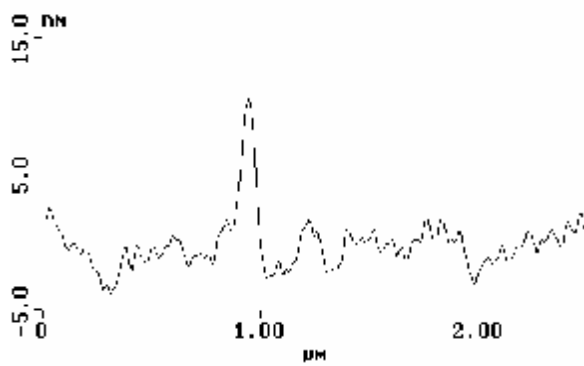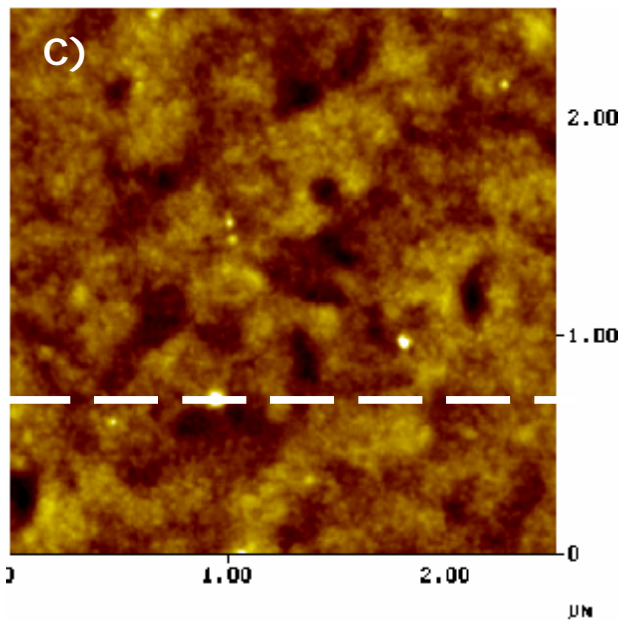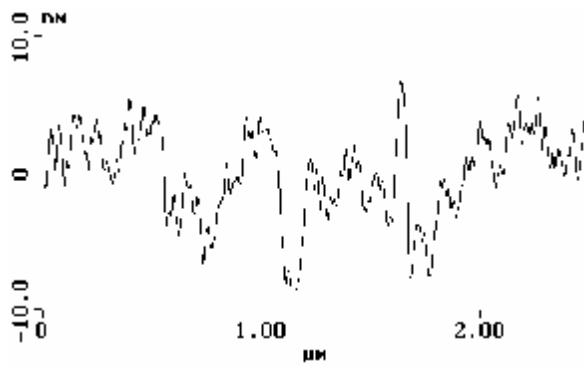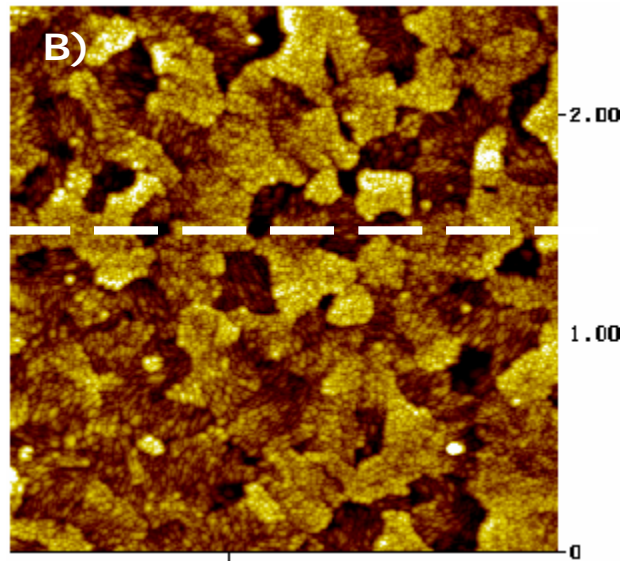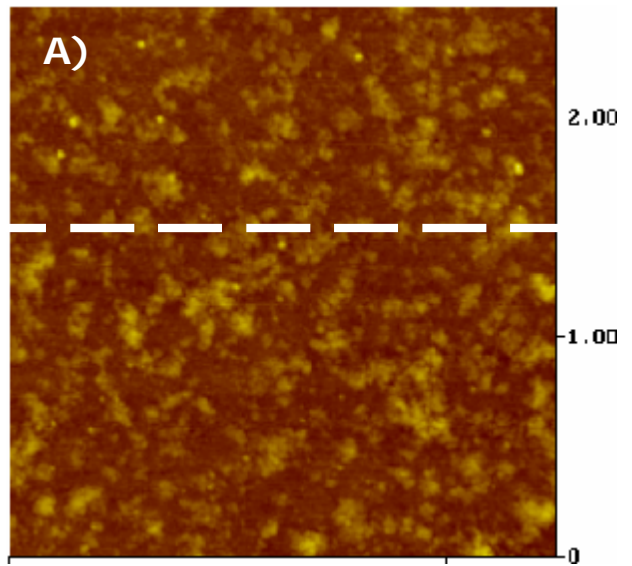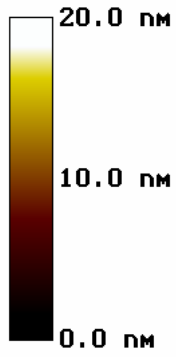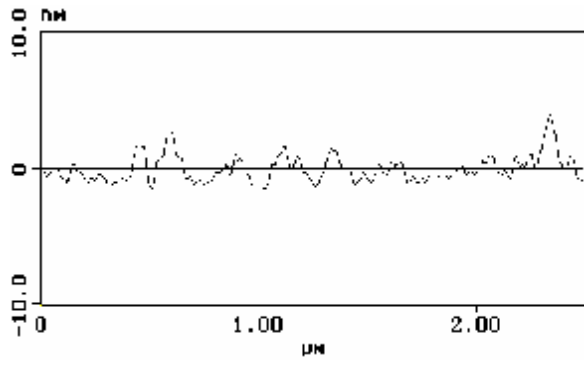
Figure 14: (previous page) AFM pictures and cross-sections: (A) a cleaned glass substrate, (B) a cleaned ITO substrate and (C) a cleaned ITO substrate after PEDOT:PSS spin-coating. The given colour code for the used height range is valid for each picture. White lines indicate the positions of the shown cross-sections.

Glass substrates have a roughness around 5 nm. The ITO substrates are rougher: 15 nm high accumulations are observed. After PEDOT:PSS spin coating the ITO / PEDOT:PSS substrate is smoother: The average roughness is 6 nm, but higher accumulations (up to 13 nm) are found all over the substrate. The nature of these accumulations was not further investigated. Similar accumulations are observed after evaporation of the active materials (following sections).

3.1.2. ZnPc films

AFM pictures and corresponding cross-sections of ZnPc films on various substrates (glass and PEDOT:PSS on ITO) deposited with different rates were taken. Figure 15 shows AFM pictures of 70 nm thick ZnPc films on glass grown with different growth rates (0.04 and 0.34 nm / s):
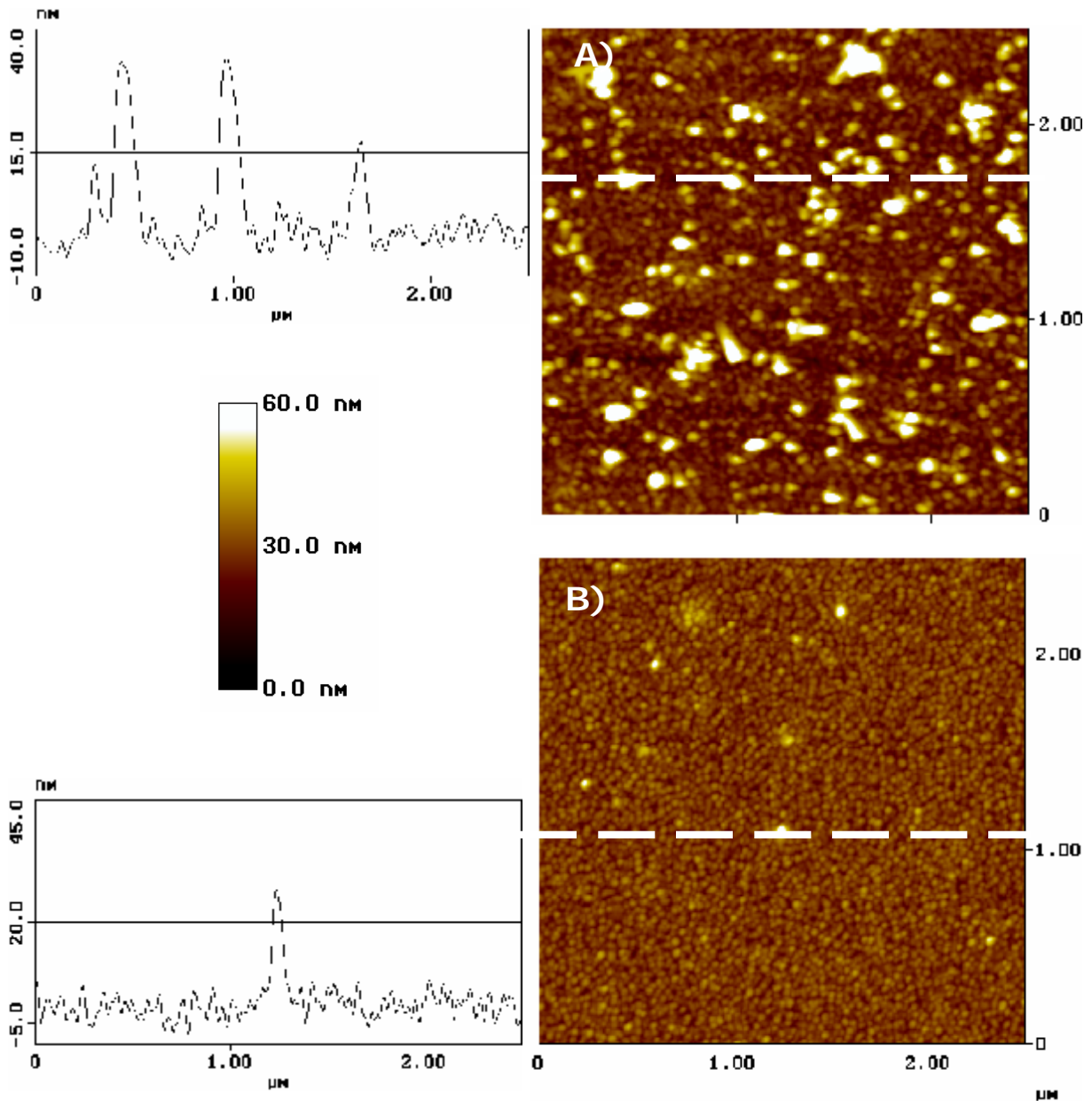
Figure 15: AFM pictures and cross-sections of 70 nm ZnPc films on glass: (A) a film grown with 0.04 nm / s, (B) a ZnPc film grown with 0.34 nm / s. The given colour code for the used height range is valid for both pictures. White lines indicate the positions of the shown cross-sections.

Slow evaporation (0.04 nm / s) leads to an average roughness around 10 nm with a lot of accumulations around 40 nm. Faster evaporation (0.34 nm / s) leads to a smoother surface (8 nm roughness) and less accumulations (around 30 nm).

Figure 16 shows AFM pictures of 70 nm thick ZnPc films on ITO / PEDOT:PSS grown with different growth rates (0.04 and 0.34 nm / s):
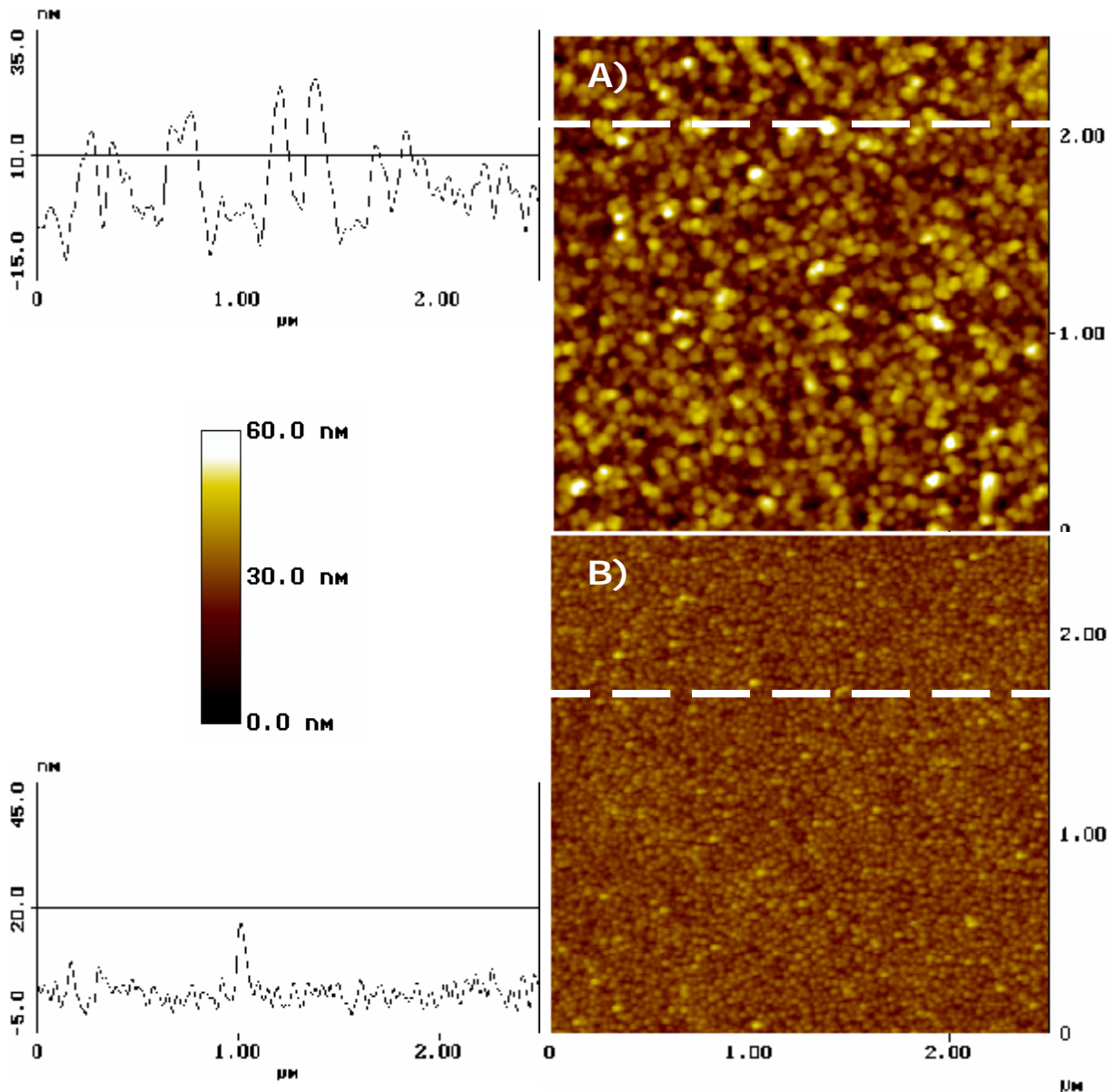
Figure 16: AFM pictures and cross-sections of 70 nm ZnPc films on ITO / PEDOT:PSS: (A) a film grown with 0.04 nm / s, (B) a ZnPc film grown with 0.34 nm / s. The given colour code for the used height range is valid for each picture. White lines indicate the positions of the shown cross-sections.

On ITO / PEDOT:PSS similar ZnPc structures as on glass are observed: Slow evaporation results in a rougher film with many high accumulations and clusters of about 70 nm average diameter. Fast evaporation causes a smoother surface with fewer accumulations and clusters of about 30 nm average diameter.

3.1.3. C_{60} films

AFM pictures and corresponding cross-sections of C_{60} films on various substrates (glass and PEDOT:PSS on ITO) deposited with different growth rates were taken. Figure 17 shows AFM pictures of 70 nm thick C_{60} films on glass grown with different growth rates (0.04 and 0.31 nm / s):
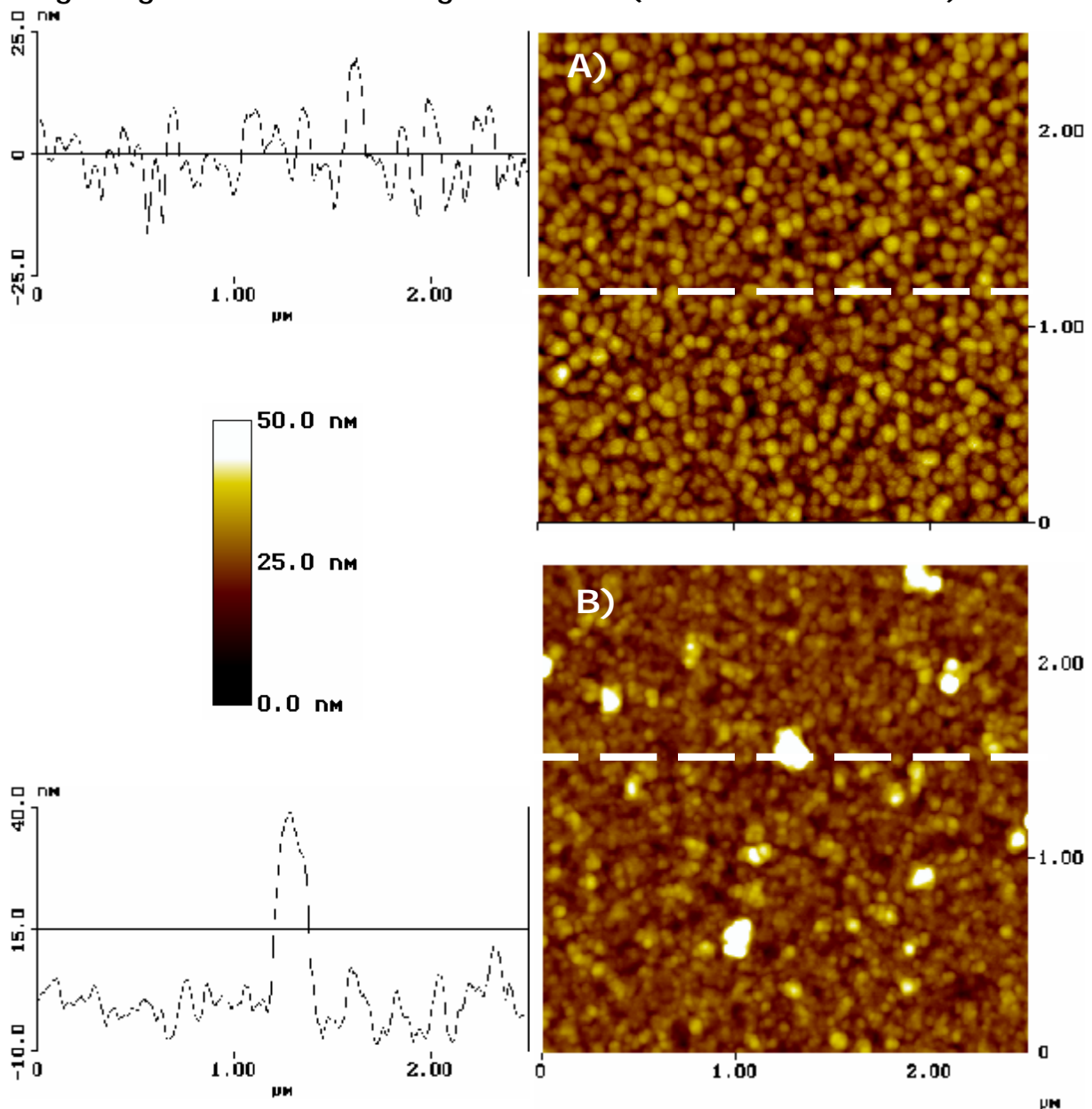
Figure 17: AFM pictures and cross-sections of 70 nm C_{60} films on glass: (A) a C_{60} film grown with 0.04 nm / s, (B) a C_{60} film grown with 0.31 nm / s. The given colour code for the used height range is valid for each picture. White lines indicate the positions of the shown cross-sections.

Figure 18 shows AFM pictures of approximately 70 nm thick C_{60} films on ITO / PEDOT:PSS grown with different growth rates (0.04 and 0.31 nm / s):
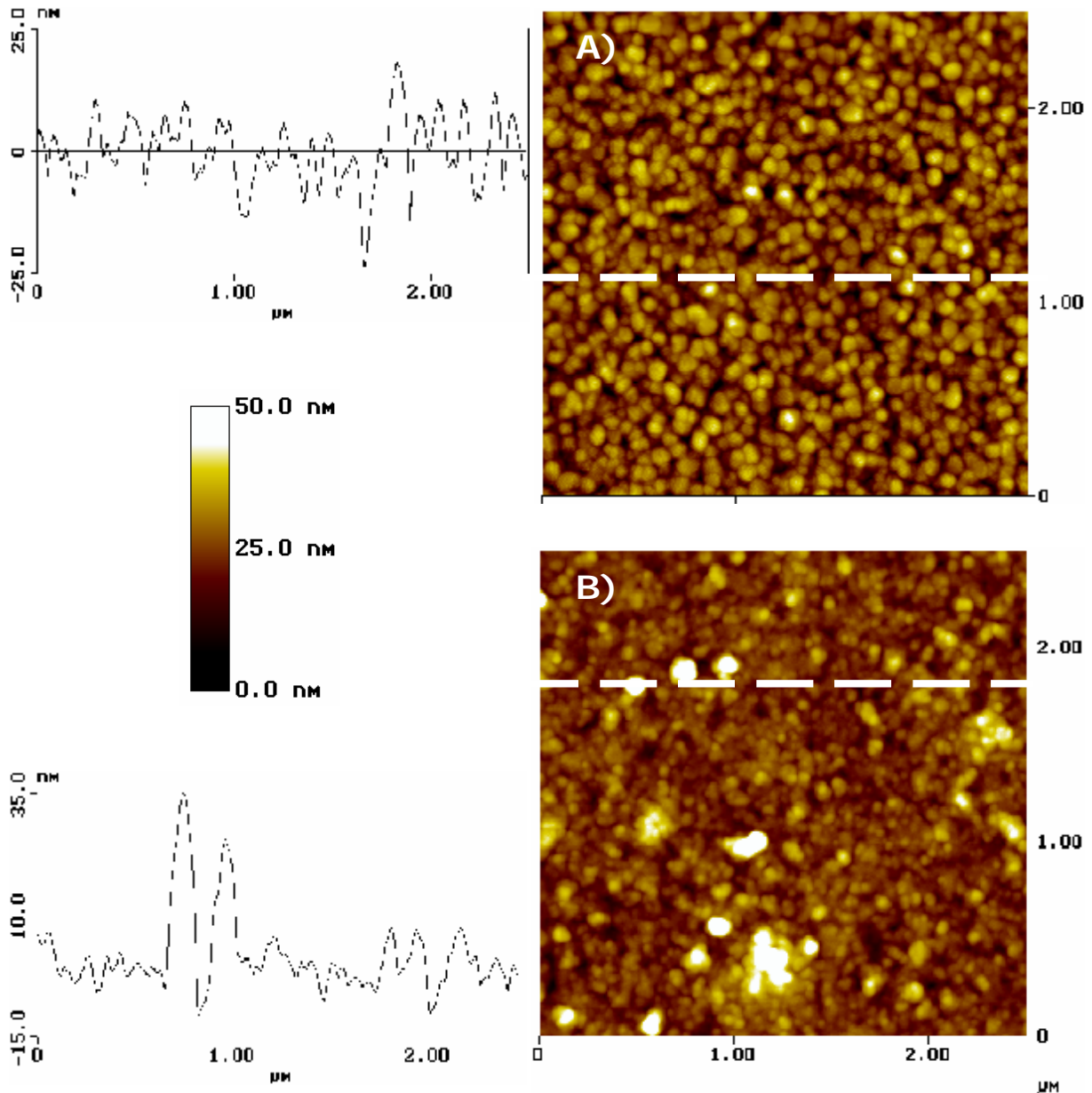
Figure 18: AFM pictures and cross-sections of approximately 70 nm thick C_{60} films on ITO / PEDOT:PSS: (A) a C_{60} film grown with 0.04 nm / s, (B) a C_{60} film grown with 0.31 nm / s. The given colour code for the used height range is valid for each picture. White lines indicate the positions of the shown cross-sections.

Slow evaporated C_{60} films on glass and as well on ITO / PEDOT:PSS are very rough (35 – 45 nm) with clusters of about 90 nm average diameter. Faster evaporation reduces the average roughness to about 20 nm with clusters of about 45 nm average diameter, but several accumulations with heights up to 45 nm remain.

3.2. UV-Vis Absorption Spectroscopy

The absorption coefficients were calculated from absorption measurements:

$$\frac{I}{I_0} = e^{-\alpha d}$$

Equation 11

I is the measured intensity, *I₀* is the standard intensity, d is the thickness of the film and α is the absorption coefficient.

The spectra give the information in which spectral range the material absorbs. Figure 19 shows the absorption coefficients of ZnPc and C_{60}:
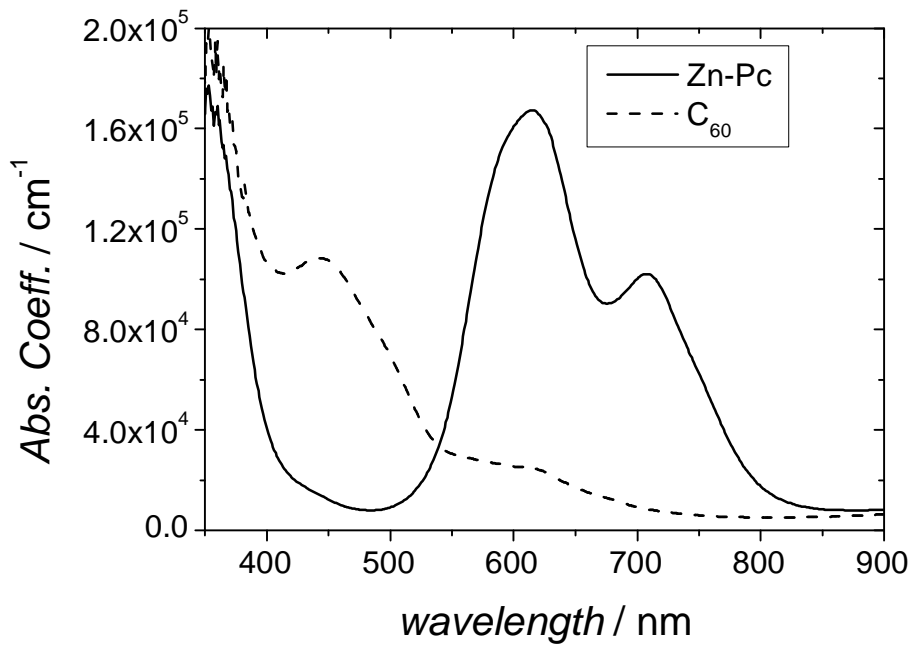
Figure 19: Absorption coefficients of ZnPc and C_{60}.

The absorption coefficients are calculated as:

$$\alpha[cm^{-1}] = \frac{1-T}{\lambda[cm]}$$

Equation 12

The spectrum of a bilayer device is the superposition of the spectra of the pure materials. This shows that there is no ground state interaction between the used materials.

3.3. Photoluminescence Measurements

Photoluminescence (PL) measurements are used to show that a material is photo-active (single layers on glass - Figure 20 A and B). In bilayer devices PL quenching is expected, if a charge transfer occurs and the layer thickness does not exceed the thickness of the active region. Figure 20 shows the PL spectra of ZnPc and C_{60} and a bilayer (illuminated from both directions) on glass.
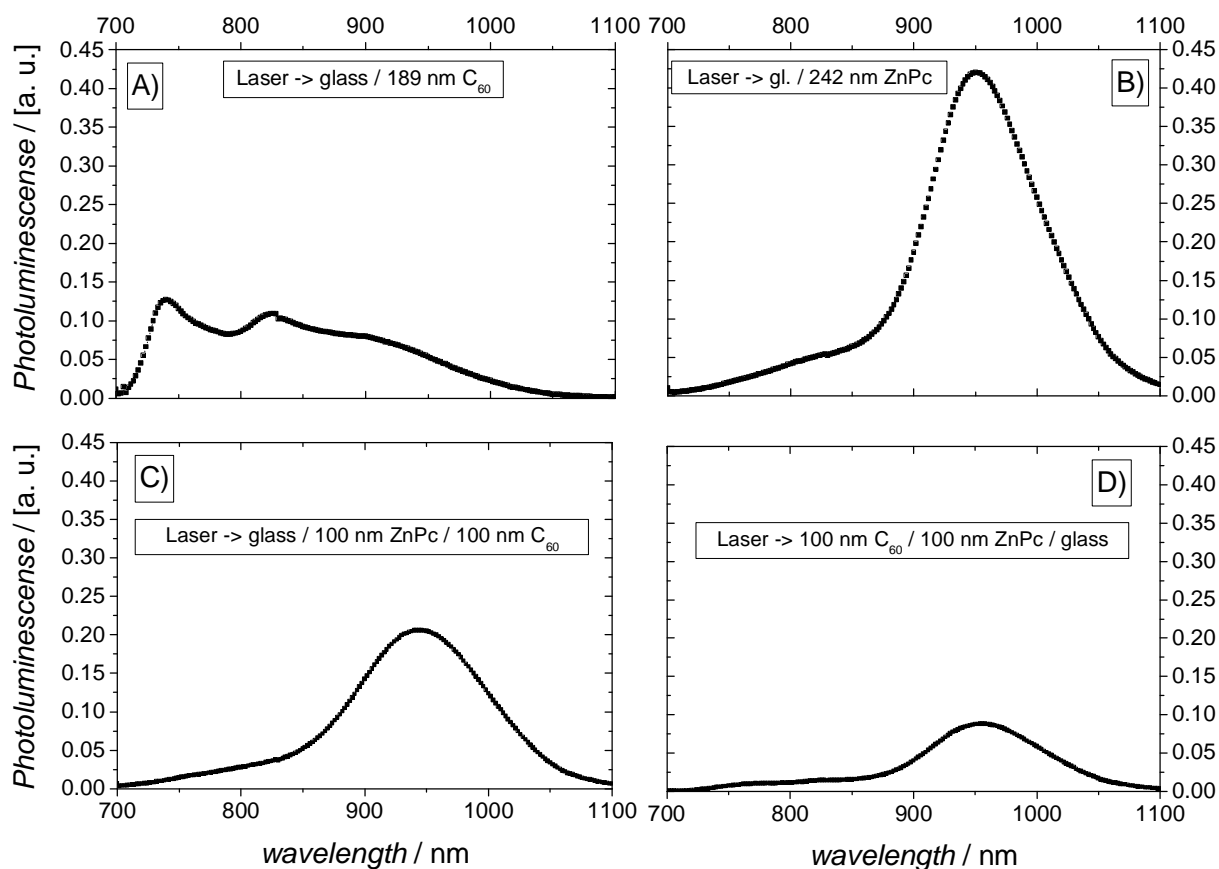
Figure 20: PL spectra @ 80 K of A) about 190 nm C_{60} on glass, B) about 240 nm ZnPc on glass and a bilayer (glass / 100 nm ZnPc / 100 nm C_{60}) illuminated C) through the glass and D) through the C_{60} layer. Excitation wavelength is 664 nm with 45 mW.

Figure 20 A) and Figure 20 B) show that the PL of ZnPc at the excitation wavelength (664 nm) is much stronger than the PL of C_{60} (compare section 3.2). In the bilayer (C) the PL signal of ZnPc is slightly reduced. The PL contribution of C_{60} is negligible because the ZnPc layer is thick enough to absorb most of the incoming light. Illumination through the C_{60} layer (D) reduces the PL signal at 740 nm by more than 90 %. For thin layers a strong reduction ("quenching") of the PL signal is expected [43, 44]. The reason is charge transfer, but the films of the investigated devices are too thick to expect luminescence quenching.

3.4.   Current-Voltage Measurements

Solar cells (preparation and structure see 2.1) with varying ZnPc thicknesses and varying C_{60} thicknesses were investigated.

The measurement of current-density (J) – voltage (V) – characteristics is an important technique for characterizing solar cells. It gives a lot of information (e. g. short – circuit current (J_{sc}), open circuit voltage (Voc), efficiency, ...) about the investigated solar cells.

3.4.1. Dark Current Behaviour

The J - V measurements in the dark were performed to check whether the device is working (diode characteristic) or short circuited and to determine the rectification ratio. The rectification ratio is defined as the absolute value of forward current (at a certain positive voltage) divided by the absolute value of the backward current (at the corresponding negative voltage). They give the important information how good the diode is. Whenever possible only devices with a rectification ratio better than 10 at ± 2 V were used for further measurements.
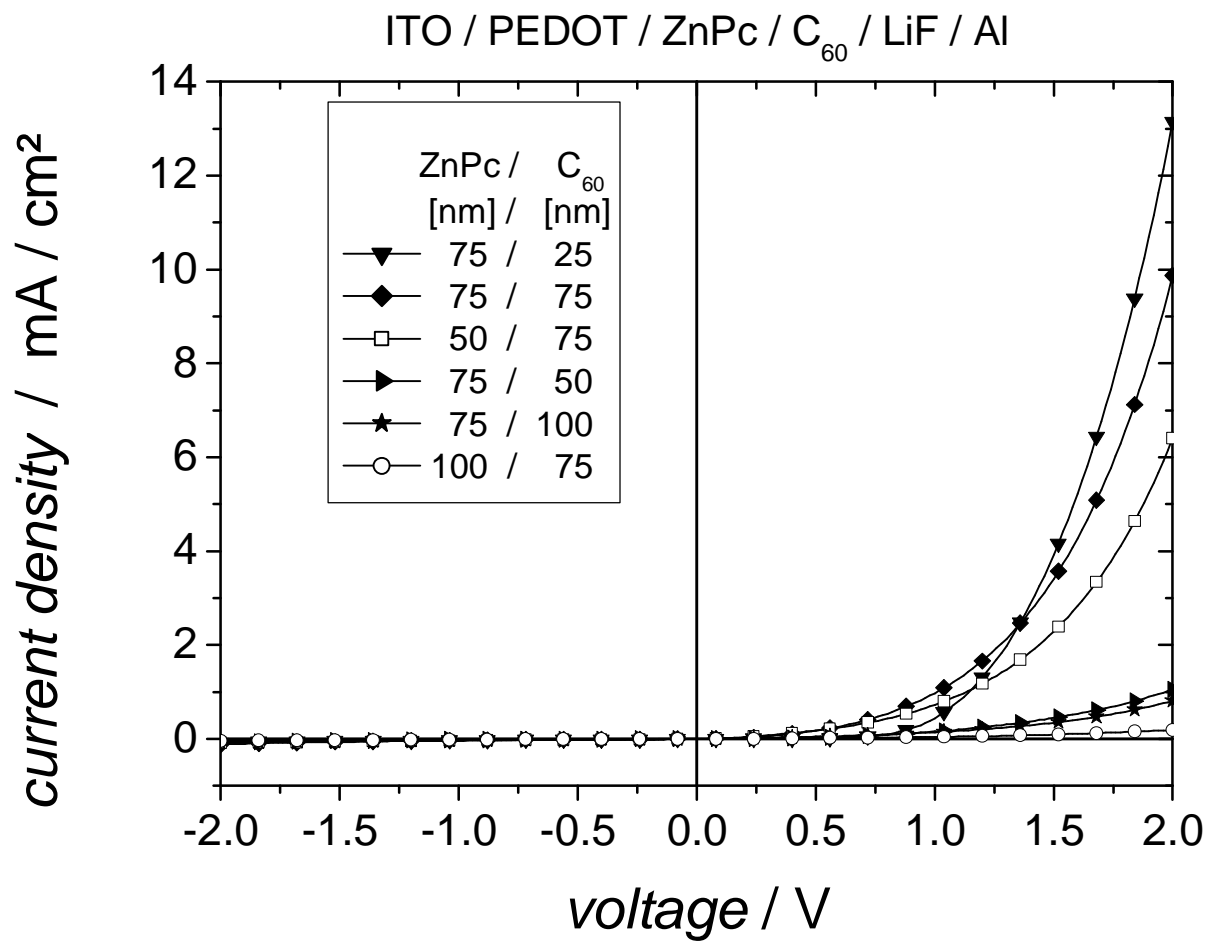
Figure 21: *J - V* characteristics in the dark of devices with varying ZnPc and C_{60} thicknesses, respectively. The investigated devices have the following structure: ITO / PEDOT:PSS / ZnPc / C_{60} / LiF / Al.
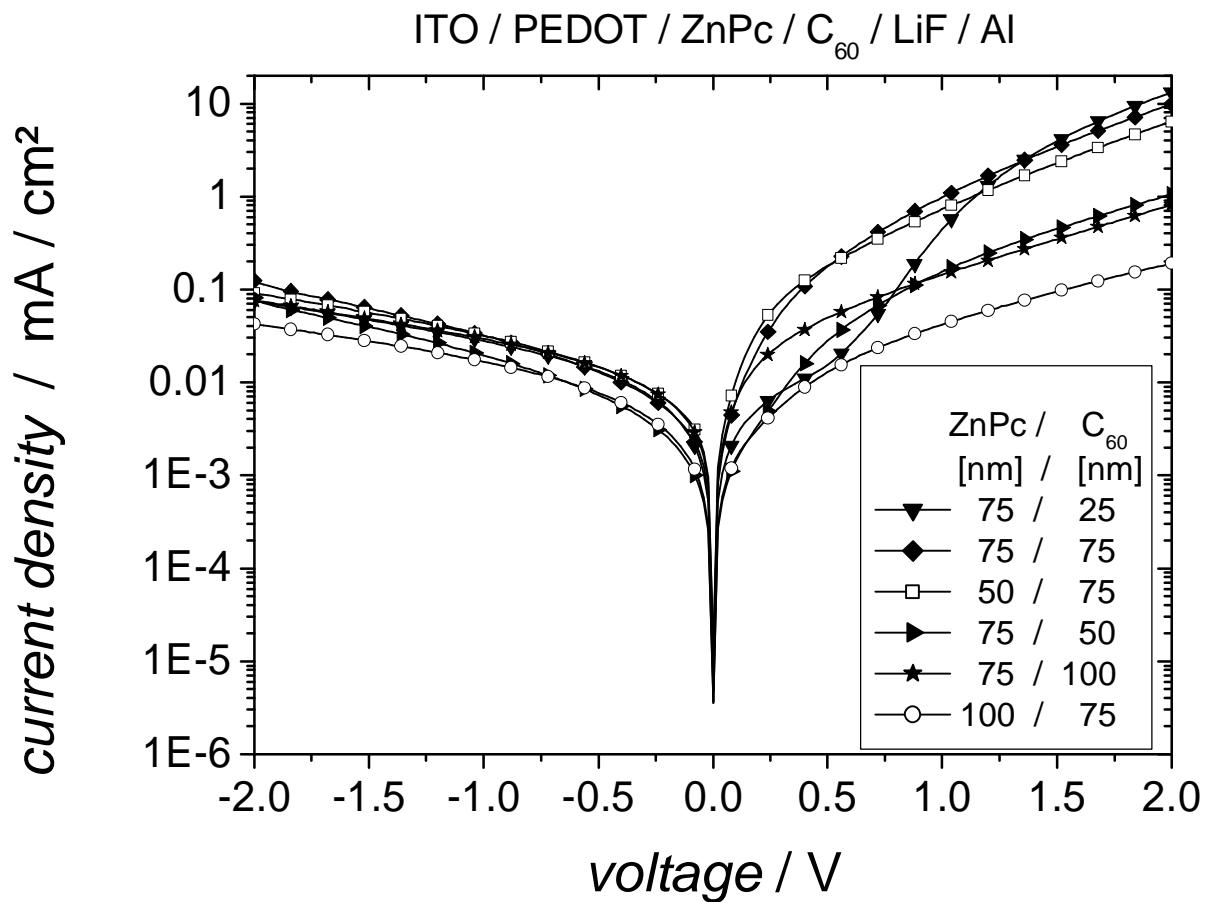
Figure 22: The same *J - V* characteristic as show in Figure 21 plotted on a logarithmic scale to determine the rectification-ratio.

Figure 21 and Figure 22 show the *J - V* characteristics of some of the investigated bilayer devices: Figure 21 uses a linear y-axis; Figure 22 uses a logarithmic y-axis where it is easier to determine the rectification ratio. Table 1 gives the rectification ratios at $\pm$ 2 V:

Table 1: Rectification ratios of the devices shown in Figure 22.

ZnPc *thickness* / nm	C_{60} *thickness* / nm	rectification ratio
75	25	153
75	75	70
50	75	62
75	50	12
75	100	9.7
100	75	4.1

A general rule whether the rectification ratio depends on the ZnPc and / or on the C_{60} thickness was not observed. (See also 3.4.5: Reproducibility)

3.4.2. Photocurrent Behaviour

Figure 23 shows a typical *J - V* characteristic of a device as investigated:
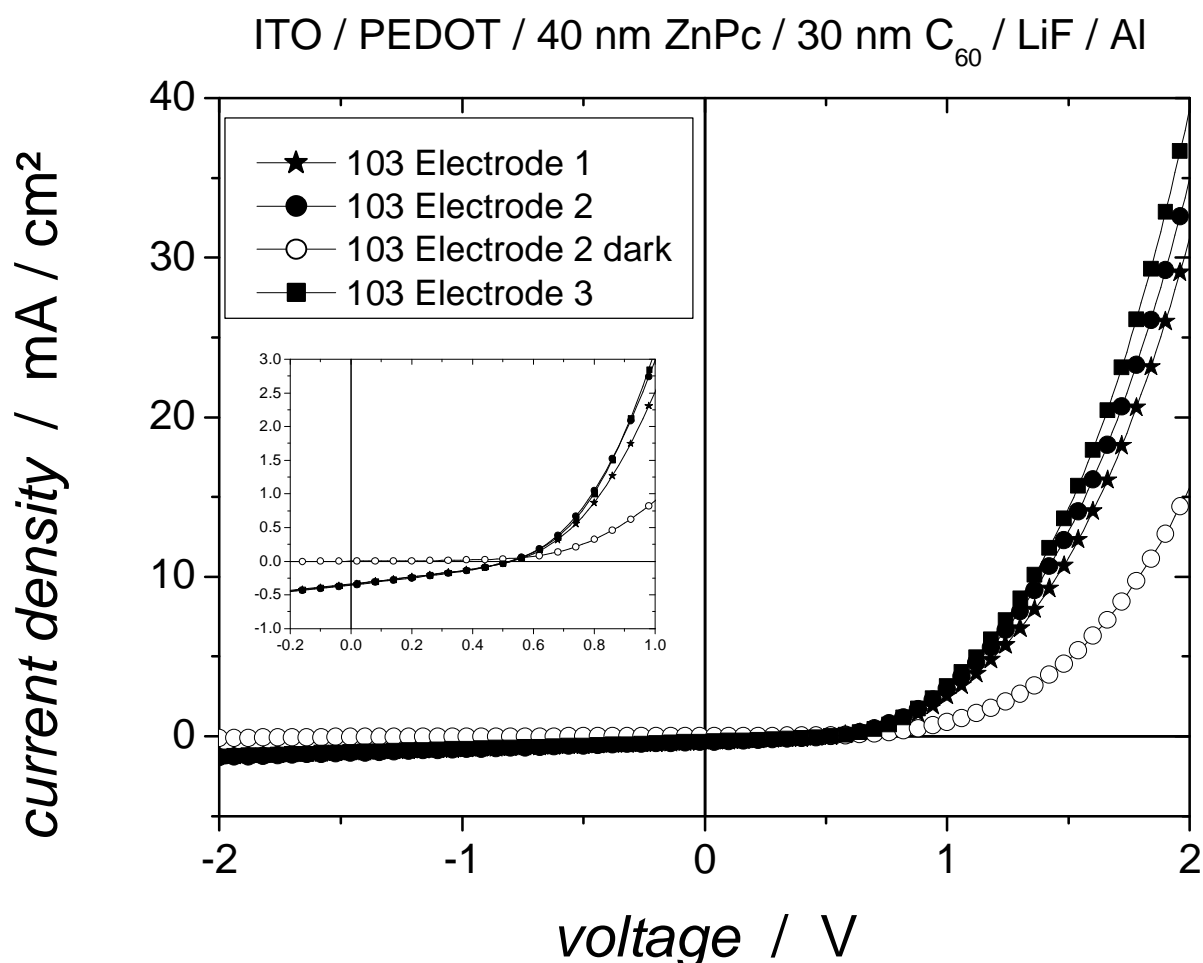
Figure 23: Illuminated *J - V* characteristic of a ZnPc / C_{60} device (see figure – heading for structure) using three parallel top-electrodes and the dark *J - V* characteristic of the middle top-electrode (electrode 2). The insert gives a closer look at the fourth quadrant.

For this device the rectification ratio under illumination at $\pm$ 2 V is in a range of 25 to 31, the rectification in the dark is 143. The photocurrent curves cross the dark current curve a few mV after the V_{oc}.

The *FF* of this device is with 0.29 in the lower range compared to other devices that reached up to 0.4. A V_{oc} of 540 mV was not often observed: The average V_{oc} was in a range of 220 to 360 mV. The highest observed

V_{oc} (600 mV) was measured for a 75 nm ZnPc / 25 nm C_{60} device. The J_{sc} is in a range of 0.34 to 0.36 mA / cm², which is one of the lowest observed. The highest J_{sc} (2.22 mA / cm²) was measured for a 50 nm ZnPc / 75 nm C_{60} device.

In the following sections, devices with varying ZnPc (section 3.4.3) or varying C_{60} (section 3.4.4) thickness will be compared.

3.4.3. Varying the ZnPc thickness

Varying the ZnPc thickness seems to influence the V_{oc} (Figure 24), but reproducibility problems (section 3.4.5) have to be taken into account. Therefore it cannot clearly be stated that the ZnPc thickness influences the V_{oc}. In contrast to V_{oc}, the J_{sc} is clearly thickness dependent (Figure 25): J_{sc} decreases with increasing ZnPc thickness.
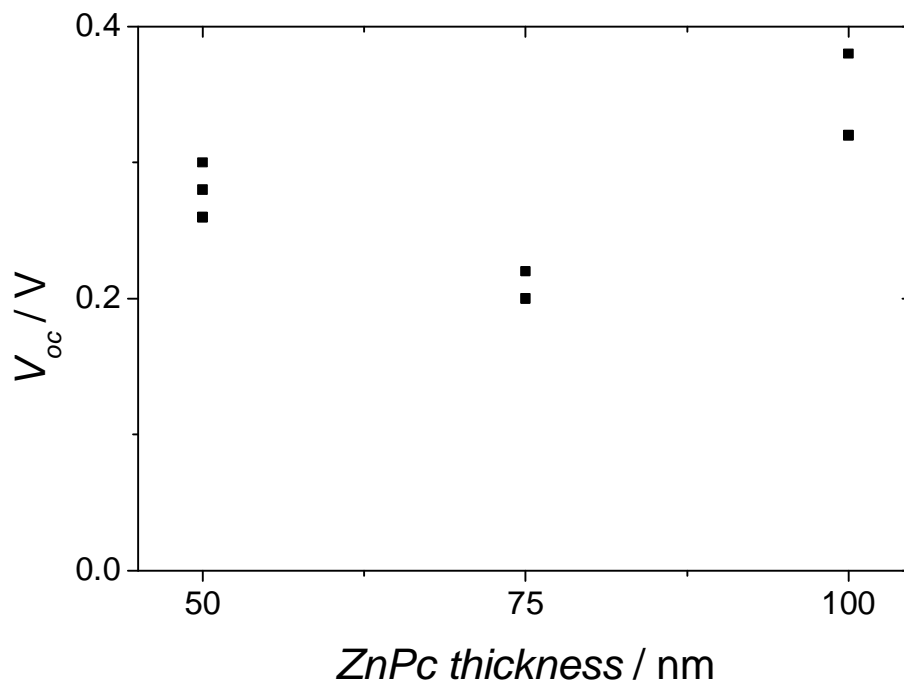
Figure 24: Effect of varying the ZnPc – thickness in ITO / PEDOT / ZnPc / 75 nm C_{60} / LiF / Al devices on V_{oc}.
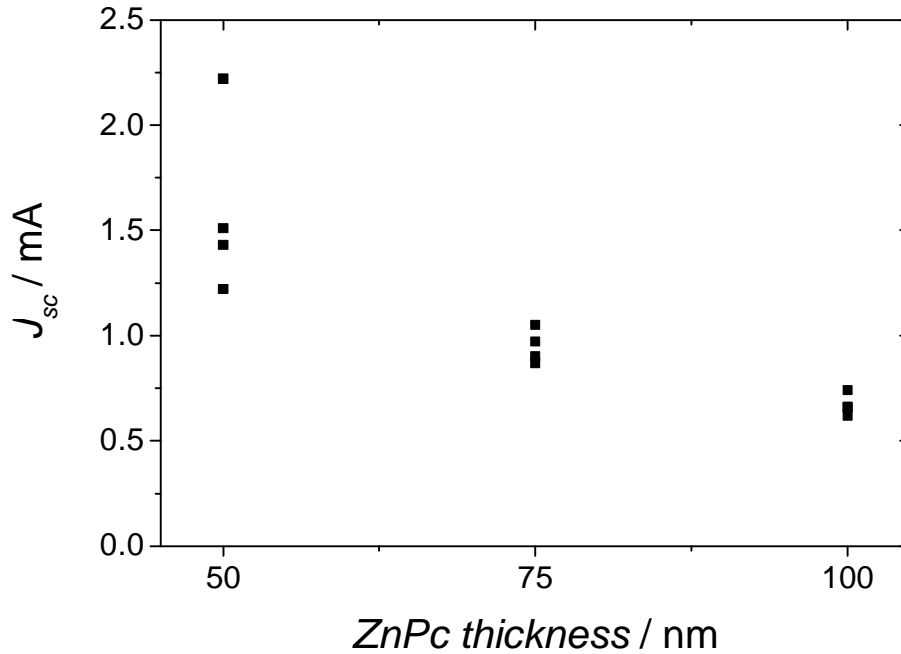
Figure 25: Effect of varying the ZnPc − thickness in ITO / PEDOT / ZnPc / 75 nm C_{60} / LiF / Al devices on J_{sc}.

3.4.4. Varying the C_{60} thickness

The C_{60} thickness seems to directly influence the V_{oc}: With increasing C_{60} thickness the V_{oc} is decreasing. However, if the values for very thin C_{60} layers are not taken into account, the variation of the V_{oc} is in the same range as it is when varying the ZnPc thickness and again reproducibility has to be taken into account. For very thin C_{60} layers it is not clear whether the C_{60} film really covers the whole ZnPc film or whether there are only C_{60} islands. If the C_{60} film is not homogenous, there are ZnPc / Al interfaces next to the ZnPc / C_{60} / Al interfaces. Therefore, the V_{oc} of these devices cannot be compared to devices with thicker films.

The J_{sc} is very low for thin C_{60} films on top of ZnPc films. For films thicker than 40 nm the J_{sc} seems to stay constant or to slightly decrease.
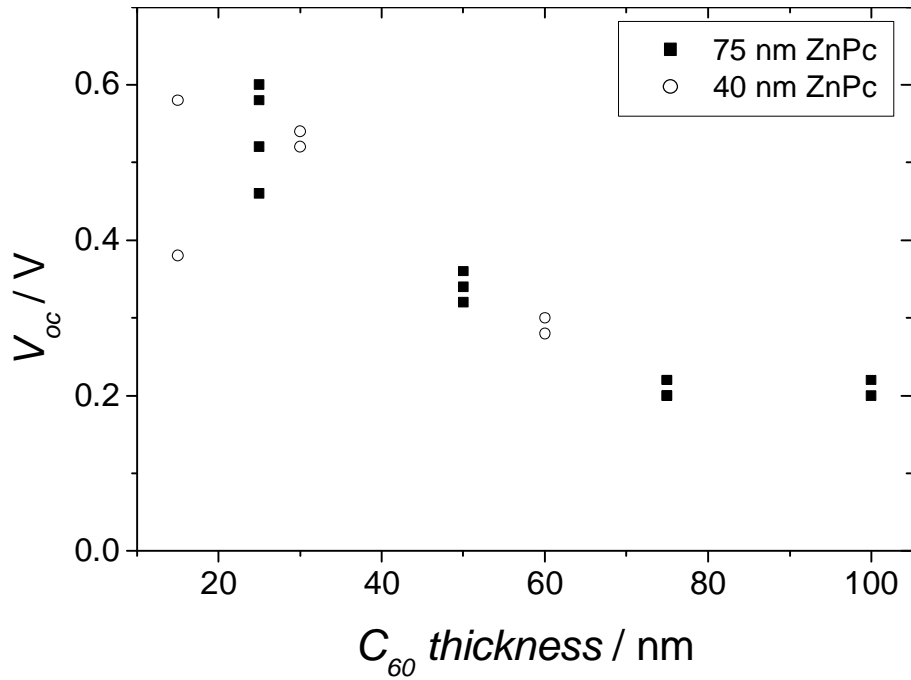
Figure 26: Effect of varying the C_{60} – thickness in ITO / PEDOT / ZnPc / C_{60} / LiF / Al devices on V_{oc}. Different devices with 40 respectively 75 nm ZnPc are investigated.
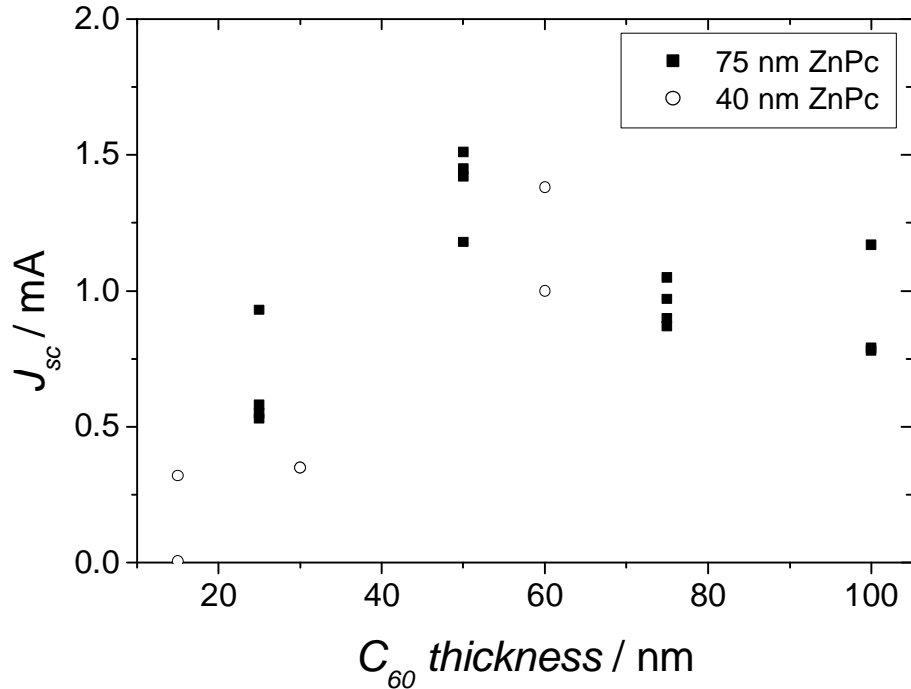
Figure 27: Effect of varying the C_{60} – thickness in ITO / PEDOT / ZnPc / C_{60} / LiF / Al devices on J_{sc}. Different devices with 40 respectively 75 nm ZnPc are investigated.

3.4.5. Reproducibility

Of this type a large number of solar cells has been produced. Many of them show the "typical" *J - V* curve with the "typical" shape which was already shown in Figure 23. However many devices did not show this typical shape. More than 50 % of the devices show "back diode effects" (compare section 4.2) as shown in Figure 28:
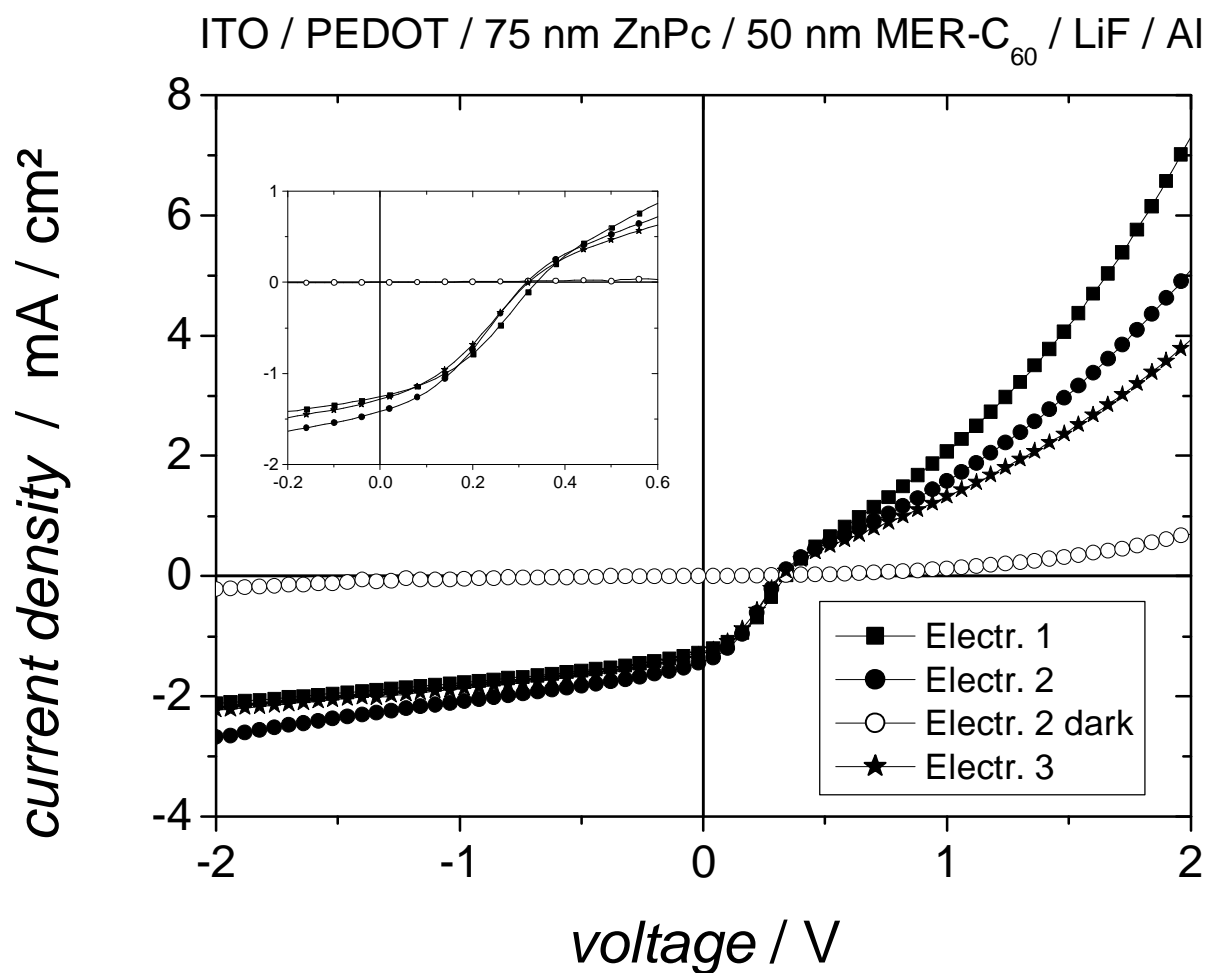
Figure 28: *J - V* characteristic (device 217) under illumination and in the dark. The heading shows the structure of the device. The insert gives a closer look to the fourth quadrant.

Possible reasons for the back diodes are problems with charge injection or extraction. Also O_2 can influence the rectification of ZnPc devices (compare section 1.3). The origin of the back diodes was not further investigated.

Figure 29 shows another device: Comparing the three parallel top electrodes shows that the J_{sc} varies between 0.7 and 1.2 mA / cm². Electrodes 1 and 2 have a much better rectification than electrode 3, which also exhibits a strong back diode.
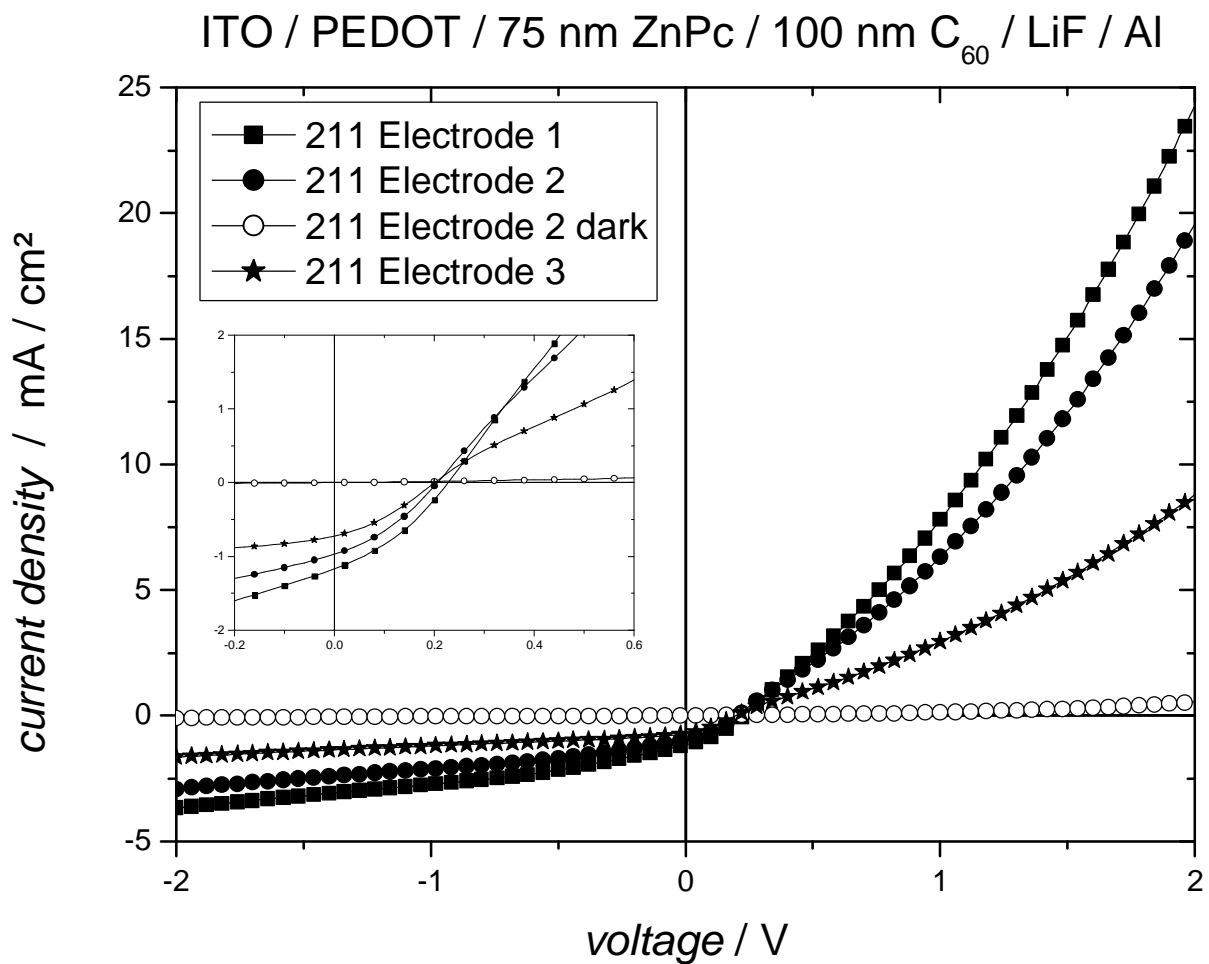
Figure 29: *J - V* characteristic of the three parallel top electrodes of device 211 under illumination and of the middle electrode in the dark.

3.5. *IPCE* Measurements

3.5.1. *IPCE* Spectra

Various devices of the structure glass / ITO / PEDOT:PSS / ZnPc / C_{60} / LiF / Al were investigated. Figure 30 shows three devices with varying thickness of the ZnPc layer. The thickness of the C_{60} layer is always 75 nm. Increasing the ZnPc thickness to 100 nm leads to a significant reduction in the *IPCE* signal.
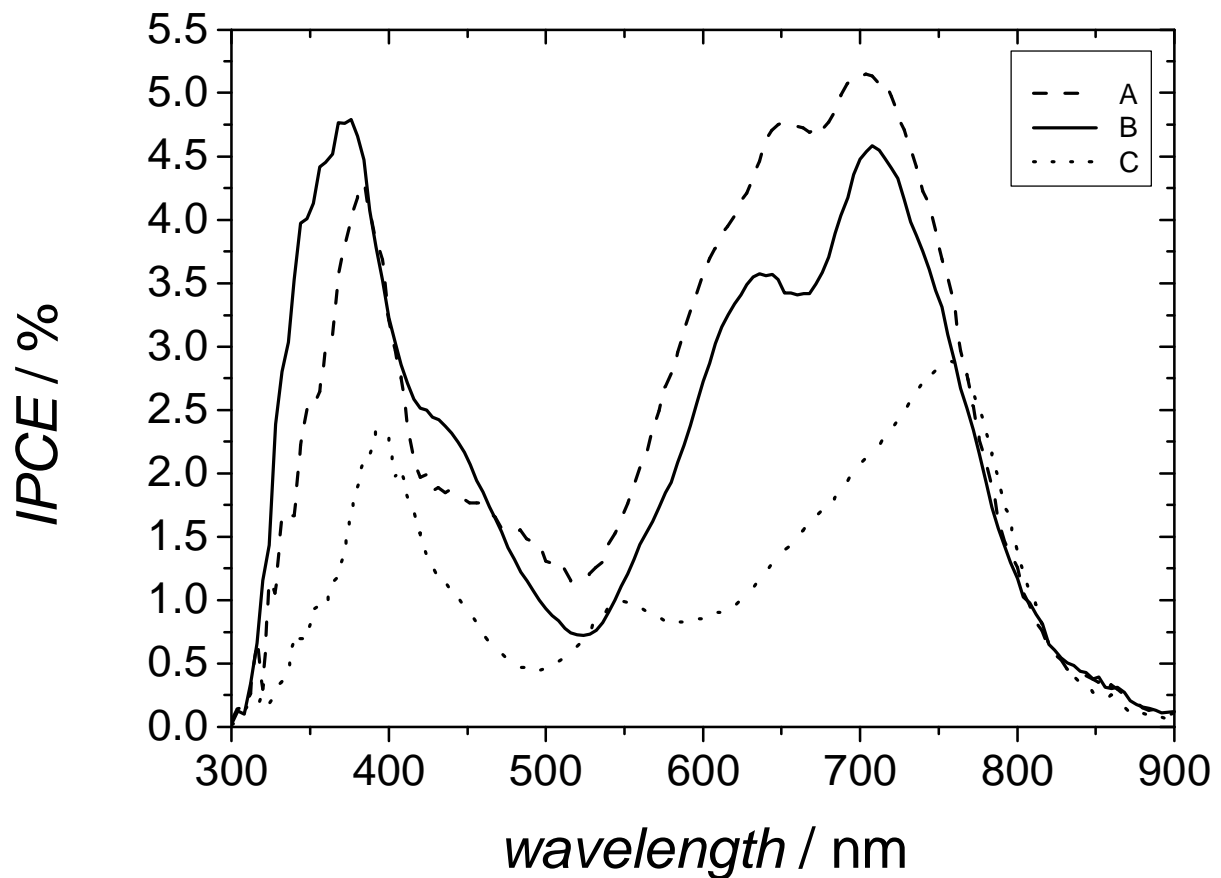
Figure 30: *IPCE* spectra of ITO / PEDOT:PSS / ZnPc / 75 nm C_{60} / LiF / Al with varying ZnPc thickness: A) 50 nm ZnPc, B) 75 nm ZnPc and C) 100 nm ZnPc.

Increasing the ZnPc thickness reduces the intensity and the peak maxima between 500 and 800 nm are shifted (see section 4.4: filter effect).
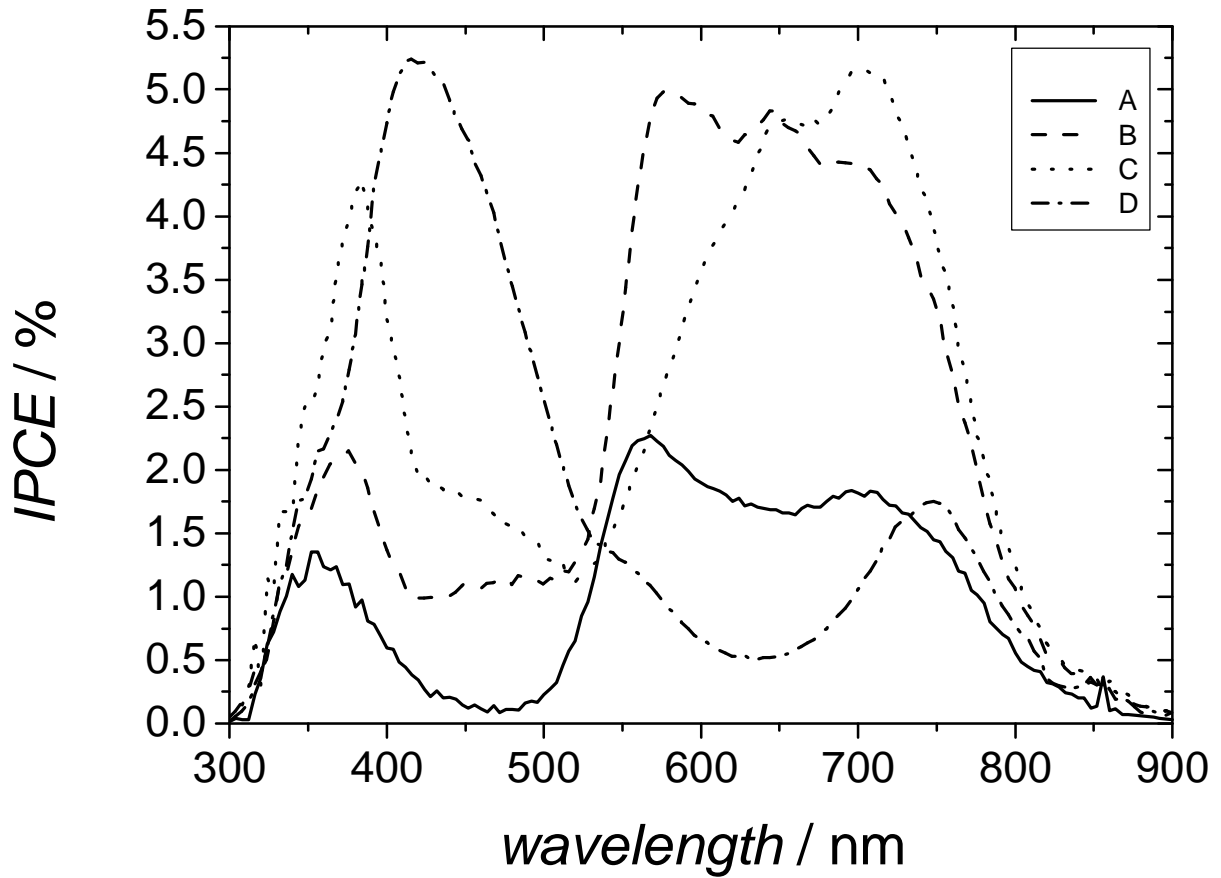
Figure 31: *IPCE* spectra of ITO / PEDOT:PSS / 75 nm ZnPc / C_{60} /LiF / Al with varying C_{60} thickness: A) 25 nm C_{60}, B) 50 nm C_{60}, C) 75 nm C_{60} and D) 100 nm C_{60}.

Figure 31 shows *IPCE* spectra of devices with the structure glass / ITO / PEDOT:PSS / 75 nm ZnPc / C_{60} / LiF / Al. The thickness of ZnPc is kept constant, while the C_{60} thickness varies from 25 to 100 nm. Devices with 25 nm of C_{60} show the weakest *IPCE* signal. Increasing the C_{60} thickness to 50 or 75 nm leads to an increase of the *IPCE* signal. Further increase of the C_{60} layer to 100 nm increases the spectrum around 450 nm (the region where C_{60} absorbs) but decreases heavily the range between 550 and 700 nm (where the major part of the photocurrent is produced).

3.5.2. Voltage Dependency of the *IPCE* Spectra

The voltage dependent spectra were measured using a power supply unit in series to the lock-in and to the device as described in 2.6. Figure 32 shows the voltage dependent *IPCE* spectra of a device with about 60 nm ZnPc and about 70 nm C_{60}. The V_{oc} of the investigated device is 340 mV. Starting at +200 mV the voltage is decreased to 0 mV, afterwards negative voltage is increased up to 2500 mV. Doing this, the maxima of the spectrum do not change, but the photocurrents increase steadily.
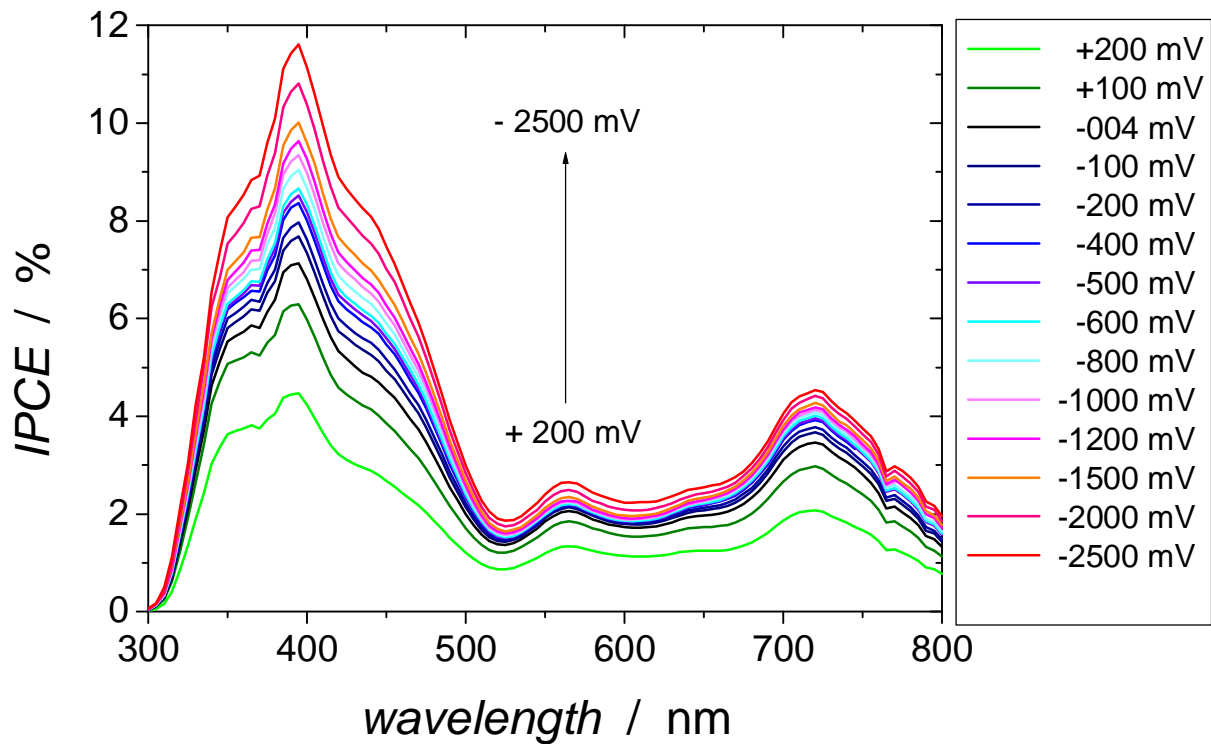
Figure 32: *IPCE* spectra with applied voltage of the following device: glass / ITO / PEDOT / about 60 nm ZnPc / about 70 nm C_{60} / LiF / Al.

Figure 33 shows *IPCE* spectra with the applied positive voltage below and above V_{oc}:
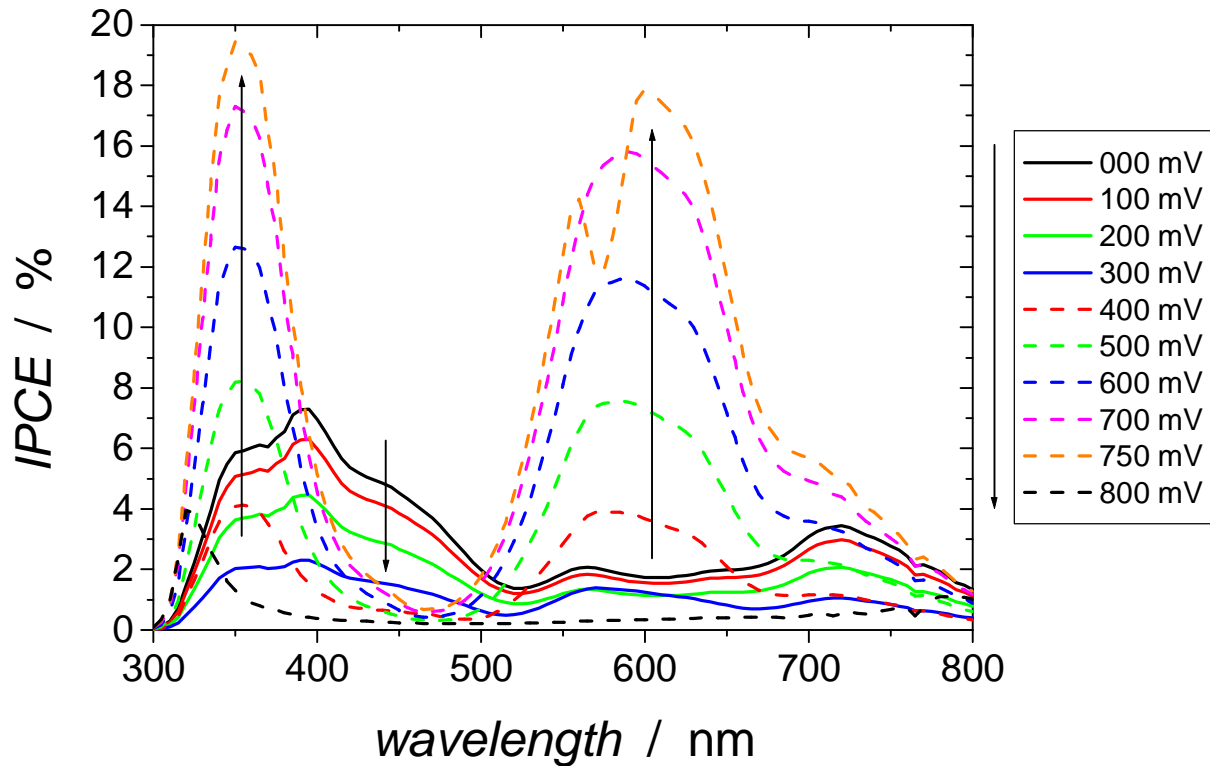
Figure 33: *IPCE* spectra with applied voltage of the following device: glass / ITO / PEDOT / about 60 nm ZnPc / about 70 nm C_{60} / LiF / Al. The voltage is applied in the fourth quadrant from 0 mV to 800 mV.

Approaching V_{oc} (340 mV) the photocurrents decrease. At higher voltages than V_{oc} the photocurrents increase again, but the spectrum has changed. The intensity of the new spectrum increases by further increasing the voltage. Reaching + 800 mV the spectrum is gone. Decreasing the voltage brings back the spectrum, showing that the process is reversible and not due to device failure.

4 DISCUSSION

4.1.   The Models

As mentioned before (1.4.4), there are two competing models in the literature about the working principle of organic bilayer solar cells: The exciton-diffusion model (section 1.4.4) and the space-charge-region model (section 1.4.3). In the exciton-diffusion model the absorbed photon creates a bound electron-hole pair, the exciton. This (electrically neutral) exciton can diffuse in all directions. If the exciton reaches by chance the p / n interface the electron and the hole are separated. Afterwards charges can be collected at the electrodes.

In the space-charge-region model the Fermi energies of the p-type and of the n-type semiconductor equilibrate. This results in a space-charge-region at the p / n interface causing a potential gradient. As in classical semiconductors it is assumed, that the electric field created here is strong enough to separate the charges. Thereby all photons absorbed in this region create charges that are driven in the electric field of the space charge region and thereby contribute to the photocurrent.

The Gärtner model (section 1.4.3.3) predicts that the photocurrent is proportional to the thickness of the space-charge-region which again is proportional to the square root of the applied voltage (Equation 6). This model is only valid if the penetration depth of the incoming light is much larger than the thickness of the active region. The penetration depth for the investigated materials is in the range of 100 nm (UV-Vis measurements, section 3.2). The thickness of the space charge region in ZnPc is calculated to be 5 nm [23]. An additional assumption is that the diffusion length of minority charge carriers (or of excitons) is much smaller than the thickness of the active region. Otherwise the contribution of diffusion (which does not depend on an applied voltage) has to be added to the photocurrent.

4.2.   Pre-conditions

An important pre-condition of the Gärtner model is that the interfaces between the layers are perfectly flat. The main technique to investigate the layer surface and thereby the structure of a device is to measure an AFM picture (section 3.1). The AFM pictures give information about the surface roughness. If the thickness of a layer is known it can be estimated whether the film covers the whole device or whether there are only islands of the material. It can be concluded that 50 nm thick films really cover the whole device. For 20 nm thick films it has to be assumed that there are holes in the film.

The AFM images of the ZnPc films (Figure 15 and Figure 16) and of the C_{60} films (Figure 17 and Figure 18) show clusters of similar size at the surface. Rostalski [6] identified ZnPc films with similar clusters as multicrystalline films. Increasing the evaporation rate from 0.01 nm / s to 0.3 nm / s results in smaller clusters and a smoother surface, i.e. about 10 nm surface roughness with many larger clusters (> 70 nm) for slowly and about 8 nm with very few larger crystallites for faster evaporated films (chapter 3.1.2). Therefore a nearly smooth interface can be assumed at least for the faster evaporated films.

Another important question is reproducibility: The reproducibility of $J - V$ curves was already discussed in section 3.4.5: In general, the $J - V$ curves are reproducible, but some show strong variations in shape, V_{oc} and J_{sc}. A big problem are back diodes: Over 50 % of the produced devices show back diodes in their $J - V$ characteristic. It can be assumed that there are two diodes of opposite direction in the device. The $J - V$ characteristic shows the linear combination of the two diodes. This means that at higher voltages than V_{oc}, where the diode should open, the second diode blocks and later breaks down. The $J - V$ characteristic shows in this region the block or the break down of the second diode.

Possible reasons for the back diodes are problems with charge injection or extraction. Also O_2 can influence the rectification of ZnPc devices (compare section 1.3), and there might be Schottky diodes at the metal / semiconductor interface. The origin of the back diodes was not further investigated.

In theory the $J - V$ curve under illumination should be given simply as the sum of the $J - V$ curve in the dark and a potential independent photocurrent. Therefore, the $J - V$ curve under illumination theoretically approaches the $J - V$ curve in the dark in forward bias, when the photocurrent is lost by recombination, but the curves should not cross. However, the curves under illumination and in the dark of all the devices investigated do cross (Figure 23). The reason for this is photoconductivity (see also section 4.5): Illumination increases the number of majority charge carriers in the device. This results in a much steeper increase of the forward current, but also in the reverse current.

The reproducibility also has to be taken into account when the *IPCE* is investigated: Figure 34 shows various *IPCE* spectra. Devices shown in one graph were built during the same production steps and thus should have the same structure. As can be seen from Figure 34 B, the variation can be quite significant.

A possible reason for the strong variations in the *IPCE* spectra observed in some cases might be that there are slight variations in the layer thicknesses. The difference between the real layer thickness and the thickness indicated by the quartz crystal thickness monitor can vary by around ± 5 %.

Optical modelling (see also section 4.4) shows that for some layer-thickness-combinations already a slight change in the thickness of one layer can cause a pronounced change in the shape of the *IPCE* spectrum.
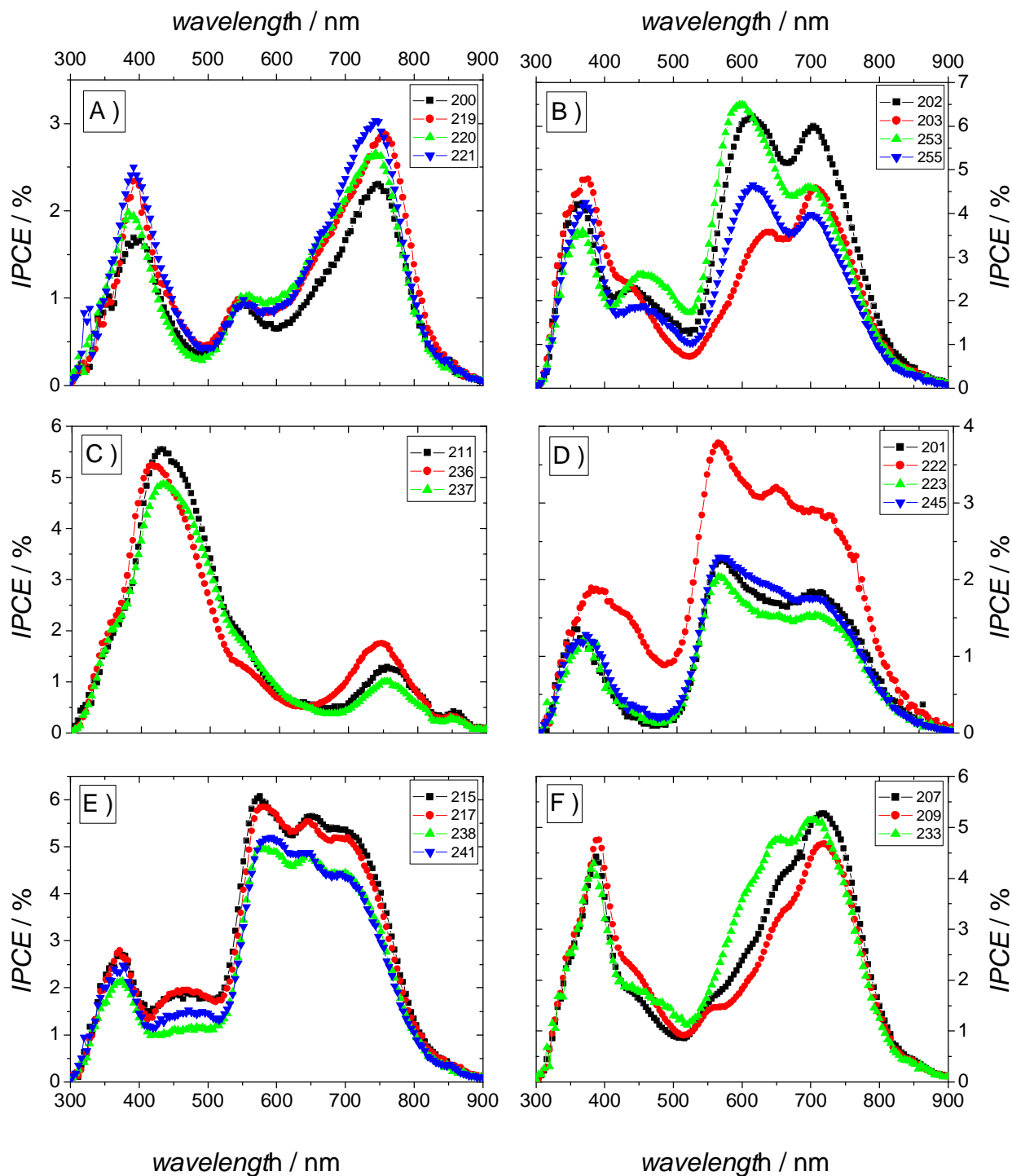
Figure 34: *IPCE* spectra of ITO / PEDOT:PSS / ZnPc / C_{60} / LiF / Al devices. The reproducibility is investigated: All devices in one graph have the same structure and were built the same way. A) 100 nm ZnPc / 75 nm C_{60}, B) 50 nm ZnPc / 75 nm C_{60}, C) 75 nm ZnPc / 100 nm C_{60}, D) 75 nm ZnPc / 25 nm C_{60}, E) 75 nm ZnPc / 50 nm C_{60} and F) 75 nm ZnPc / 75 nm C_{60}. The legends show the device numbers.

4.3.   Photocurrent

Investigating the thickness dependence of the $J - V$ characteristics shows that the J_{sc} has a maximum if the ZnPc layer is 50 nm thick (Figure 25). Varying the C_{60} thickness shows that the C_{60} layer has to exceed 40 nm. Whether the thickness variation influences the V_{oc} is difficult to say because the observed variations are within the range of reproducibility.

Decreasing the C_{60} thickness to about 25 nm results in a strong increase of the V_{oc} (Figure 26). A possible reason is that the C_{60} film is too thin to cover the whole surface. This would mean that there are ZnPc / Al interfaces next to ZnPc / C_{60} / Al interfaces. Therefore, the model cannot be applied to these films.

The best devices in terms of efficiency were 50 nm ZnPc / 75 nm C_{60} devices. They showed efficiencies up to 0.24 %. This is in accordance with the *IPCE* measurements: Figure 30 shows that devices with 50 nm ZnPc have higher *IPCE* than the spectra of devices with 75 or 100 nm ZnPc. Figure 31 shows that the highest *IPCE* spectra are measured for devices with C_{60} thicknesses between 50 and 75 nm.

As already mentioned above, the thickness of the active region was calculated to be in the range of 5 nm. It should be concluded that devices with 5 nm thin ZnPc layers should have the highest efficiencies. One pre-condition is the already mentioned flatness of the interfaces. Another point are interference effects: Due to the reflecting back electrode there is a kind of "standing wave" in the device. The position of the absorption maximum strongly depends on the thicknesses of all layers.

4.4. The *IPCE* spectra

Comparing the *IPCE* spectra with the absorption spectra shows, which material contributes to the *IPCE* at which wavelength (Figure 35): C_{60} contributes in the range of 300 to 500 nm. ZnPc contributes with two peaks in the range from 500 to 800 nm.
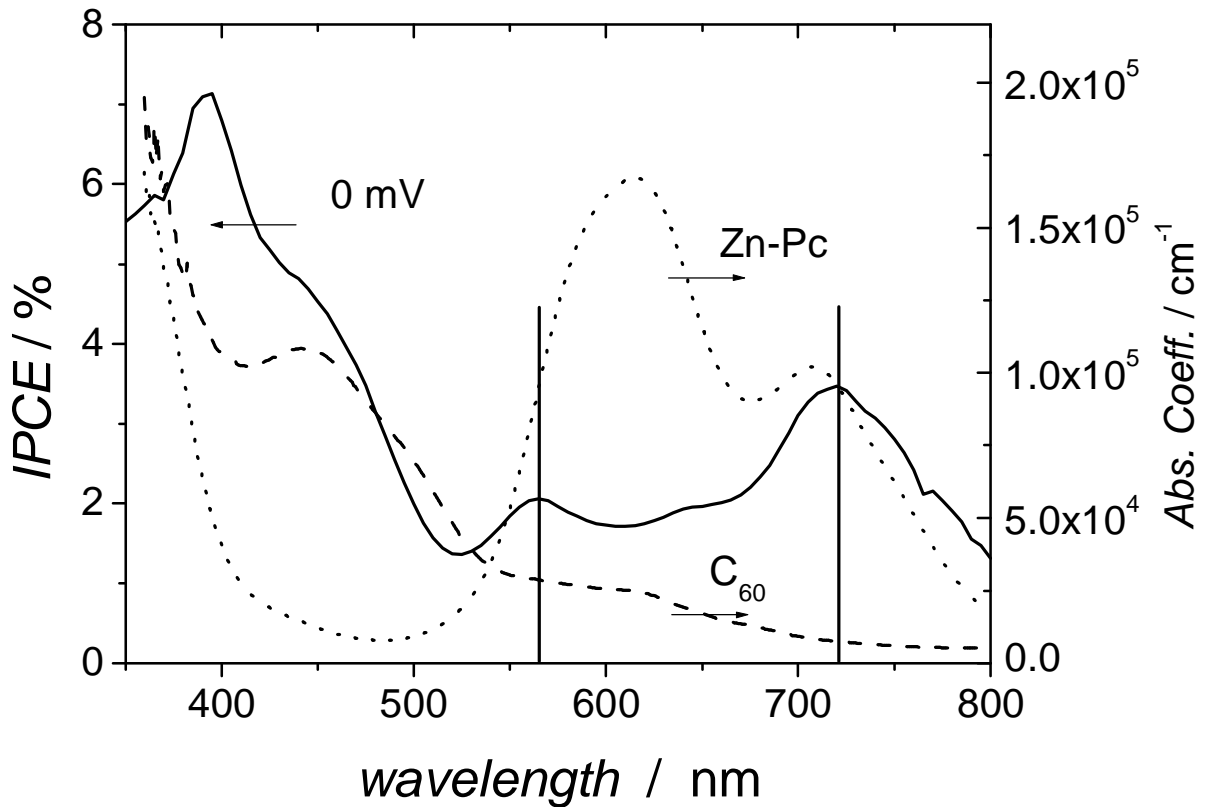
Figure 35: *IPCE* spectrum (full line, without applied voltage) of an ITO / PEDOT / about 60 nm ZnPc / about 70 nm C_{60} / LiF / Al device compared to the absorption coefficients of the materials (ZnPc dotted line; C_{60} dashed line).

Photoluminescence measurements (section 3.3) show that a large volume of the films does not contribute to the charge separation. In other words: the active area is limited to a small volume at the interface between ZnPc and C_{60}. Absorption measurements (section 3.2) show that the two materials are very strongly absorbing. The result of these two properties is a <u>filter effect</u>, which can be observed in the *IPCE* measurements:

In an optimized device the *IPCE* spectrum should have the same shape as the absorption spectrum. Considering this, from ZnPc two peaks at 615 nm and at 707 nm are expected. As already shown, ZnPc (through which the device is illuminated) is a very good absorber at this wavelength. A consequence of the thick ZnPc layer and the good absorption is that most of the light at 615 nm does not reach the active region. Therefore, there is no *IPCE* peak at 615 nm. For light with a lower absorption coefficient more photons can reach the interface and create charge carriers. Thus, *IPCE* peaks appear at the shoulders of the absorption peak. The absorption coefficients of ZnPc at the position of the two *IPCE* peaks in Figure 35 are the same (black lines).
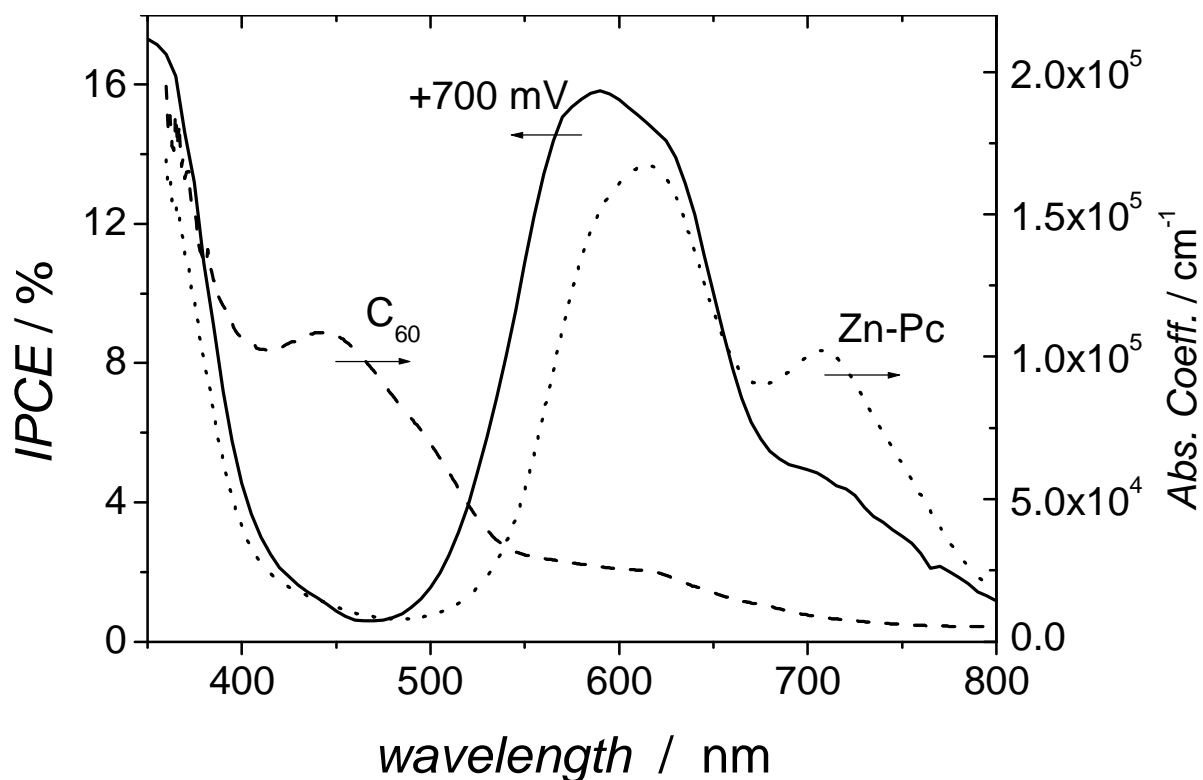
Figure 36: *IPCE* spectrum (solid line, with applied 700 mV positive voltage) of an ITO / PEDOT / about 60 nm ZnPc / about 70 nm C_{60} / LiF / Al device compared to the absorption coefficients of the materials (ZnPc dotted line; C_{60} dashed line).

Applying a positive voltage bigger than V_{oc} changes the *IPCE* spectrum. The shape of this spectrum also depends on the thickness of the ZnPc and the C_{60} layer. A possible reason for this spectral change may be strong photoconductivity. These "photoconductivity-spectra" were not investigated in detail in this thesis. However the voltage dependence of the *IPCE* maxima will be discussed in the next chapter:

Increasing the voltage to + 800 mV resulted in vanishing of the *IPCE* signal. Decreasing the voltage caused the signal to increase again. This shows that the device was still working. A possible reason for the vanishing signal is that so many majority charge carriers are injected that

the recombination rate is too high (or the lifetime too short) and thus the photogenerated minority charge carriers can not reach the electrodes.

Investigating the devices by *IPCE* measurements, a model that simulates the optical absorption within a device was investigated: Knowing the absorption profile and the thickness of the active region provides the possibility to simulate *IPCE* spectra. Earlier work showed that the model fits the experimental data well [45, 46]. In this work some *IPCE* spectra had similarities with the simulated spectra, but most of the spectra did not fit sufficiently well.

An important assumption of this model is that the interfaces between the layers are perfectly flat. As the AFM pictures show this is not the case for the devices investigated. This might be the reason for the mismatch between modelled spectra and experimental data.

4.5. Fitting the voltage dependent *IPCE*

The *IPCE* values of the measured spectra are plotted against the applied voltage. This results in a monochromatic *J - V* characteristic. Various fits (linear, exponential, logarithmic, ...) were tried for this curve. The correlation coefficients R (linear fit) and R^2 (power law fit) indicate whether the fit is good (R close to 1) or rather bad (R close to 0). The best fit is a linear fit in a log-log plot, as Figure 37 shows:

log (IPCE) = A + B * log (V_{oc} - appl.voltage)

A -1.09611   ±0.03318
B   0.44578   ±0.01188
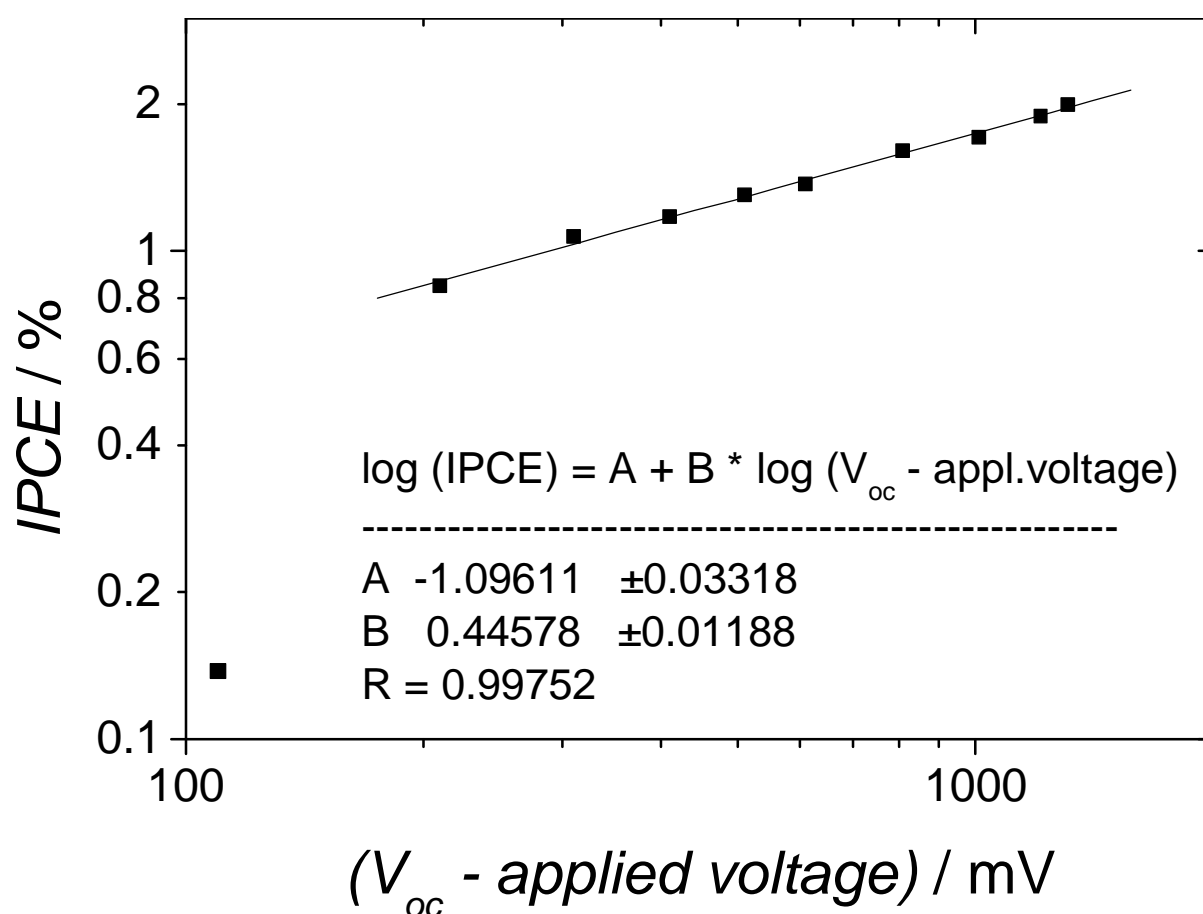R = 0.99752

Figure 37: Fit of the voltage dependent *IPCE* spectra of an ITO / PEDOT:PSS / 100 nm ZnPc / 75 nm C_{60} / LiF / Al device @ 576 nm. The first value is not included in the fit. The insert shows the fit parameter.

As explained above the *J - V* characteristics of the investigated devices under illumination and in the dark cross. Also the slope of the *J - V* curve

under illumination is stronger than the slope of the *J - V* curve in the dark (in forward and in backward direction). The reason for this behaviour is photoconductivity: Under illumination there are more charge carriers in the device. The increased number of charge carriers enables stronger injection currents.

In an ideal solar cell the *J - V* characteristic in the dark describes the behaviour of the majority charge carriers, the *J - V* characteristic under illumination describes the behaviour of majority and minority charge carriers. The *IPCE* measurement, which should be done by subtracting the *J - V* characteristic in the dark from the *J - V* characteristic under illumination, aims at investigating the contribution of minority charge carriers.

However, a result of the photoconductivity is that there are two different *J - V* characteristics of majority charge carriers: The one measured in the dark and the one upon illumination, when additional majority charge carriers are created. This leads to a theoretical *J - V* characteristic being the real *J - V* characteristic under illumination without the contribution of the minority charge carriers created by illumination, i.e. the theoretical primary photocurrent. The increase of the dark current due to additional majority charge carriers when illuminating of course changes the *J - V* characteristics very much but is not due to a real primary photocurrent; only the latter being the aim of *IPCE* investigations. Doing *IPCE* measurements the theoretical *J - V* characteristic of majority charge carriers should be subtracted from the *J - V* characteristic under illumination, which is not possible in an experiment. However, since only part of the photoeffect is due to the creation of minority charge carriers, which than is amplified by the photoconductivity, this amplification factor will occur in all *IPCE* measurements as discussed later. Only close to the V_{oc}, where the dark current with opposite sign than the primary photocurrent starts to dominate, the photocurrent can not be account for by a simple factor. The forward current here leads to the complete breakdown of the overall current. Therefore the data close to V_{oc} cannot

be taken into account for the fit. (E.g. The value at 110 mV is not used for the fit in Figure 37.)

The Gärtner model predicts that the photocurrent is proportional to the square root of the applied voltage. To investigate this model, a square root fit in a linear plot was used and the exponent was kept constant at 0.5. Figure 38 shows the fit:

IPCE = a + b * (V$_{oc}$ - appl.voltage)^c

R^2 0.99533
a   0.15223 ±0.03465
b   0.05022 ±0.0013
c   0.5   ±0
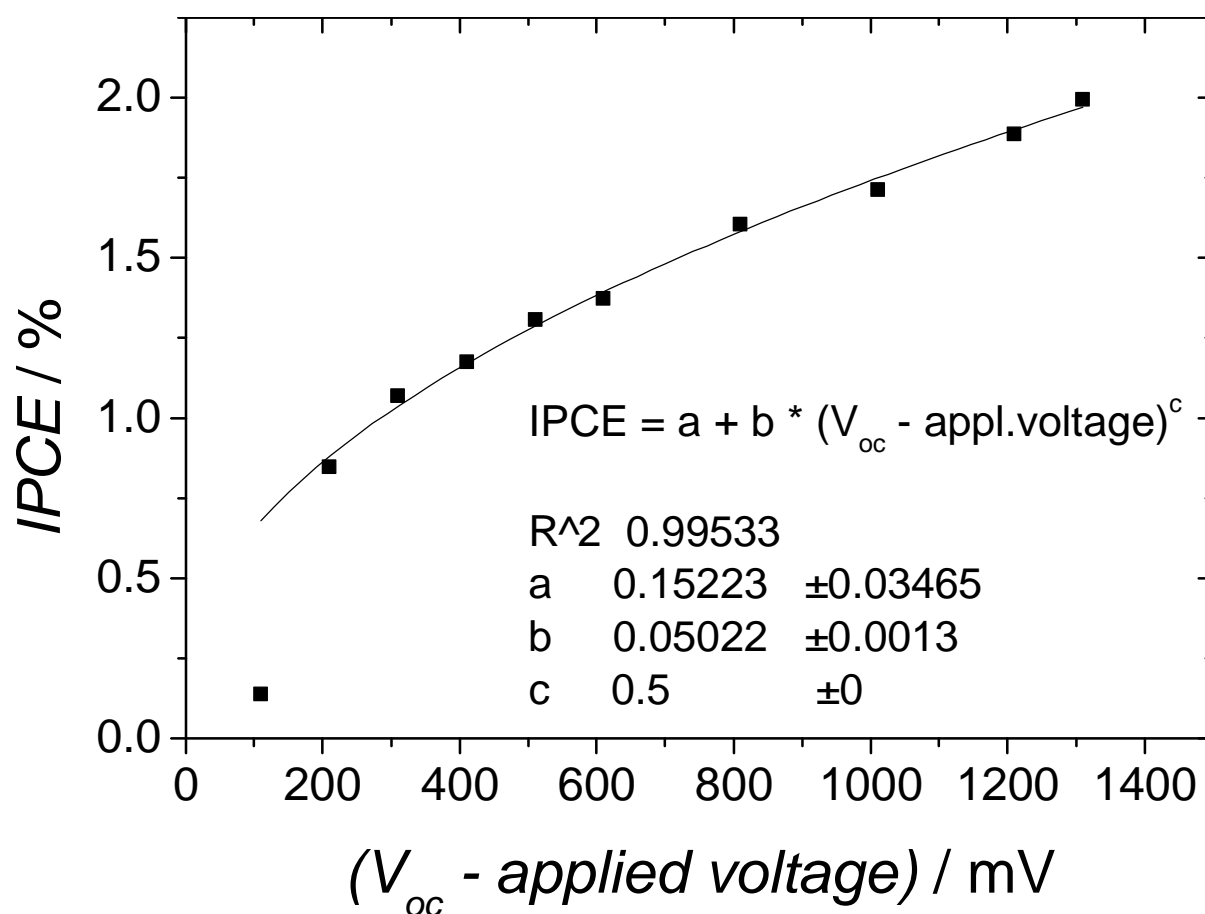
Figure 38: Fit of the voltage dependent *IPCE* spectra of an ITO / PEDOT:PSS / 100 nm ZnPc / 75 nm C_{60} / LiF / Al device @ 576 nm. The first value is not included in the fit. The insert shows the fit parameters.

As discussed above, the value next to V_{oc} is not used. In Table 2 the log-log-fit and the square root-fit for various devices are compared. For all the fits only values that are at least 200 mV more negative than V_{oc} are used.

Looking at the square root fit shows that the R² values are between 0.91 and 0.996. The prefactor "b" has values between 0.01 and 0.14. As also discussed above the reason for this prefactor < 1 is assumed to be photoconductivity: Only between 1 and 10 % of the incident light can contribute to the primary photocurrent, the rest of the light increases the photoconductivity.

Table 2:   log-log and square root fit for various devices.

device number	219	203	236	223	238	233	064	099
ZnPc thickness	100 nm	50 nm	75 nm	75 nm	75 nm	75 nm	58 nm	40 nm
C_{60} thickness	75 nm	75 nm	100 nm	25 nm	50 nm	75 nm	71 nm	60 nm
$y = a + b * x ^ 0.5$								
a	0.15	1.3	0.34	-0.6	3.18	2	1.8	0.14
b	0.05	0.03	0.04	0.14	0.19	0.06	0.009	0.06
R²	0.995	0.91	0.97	0.993	0.996	0.98	0.93	0.94
$\log(y) = a + b * \log(x)$								
b	0.45	0.18	0.36	0.59	0.3	0.2	0.05	0.42
R	0.998	0.96	0.99	0.998	0.9996	0.994	0.99	0.97

In one case even a linear behaviour was observed (Figure 39). The ZnPc layer of the investigated device was only 25 nm thick. As shown in 3.1.2 it must be assumed that such a thin film does not cover the hole device. Therefore PEDOT:PSS / C_{60} interfaces are assumed to be next to PEDOT:PSS / ZnPc / C_{60} interfaces. Such devices cannot be simulated with a simple bilayer picture. Therefore, they must be excluded from the model.

$$IPCE = A + B * (V_{oc} - appl.voltage)$$

A 1.21706 0.03398
B 0.0024 3.57464E-5
R 0.99901
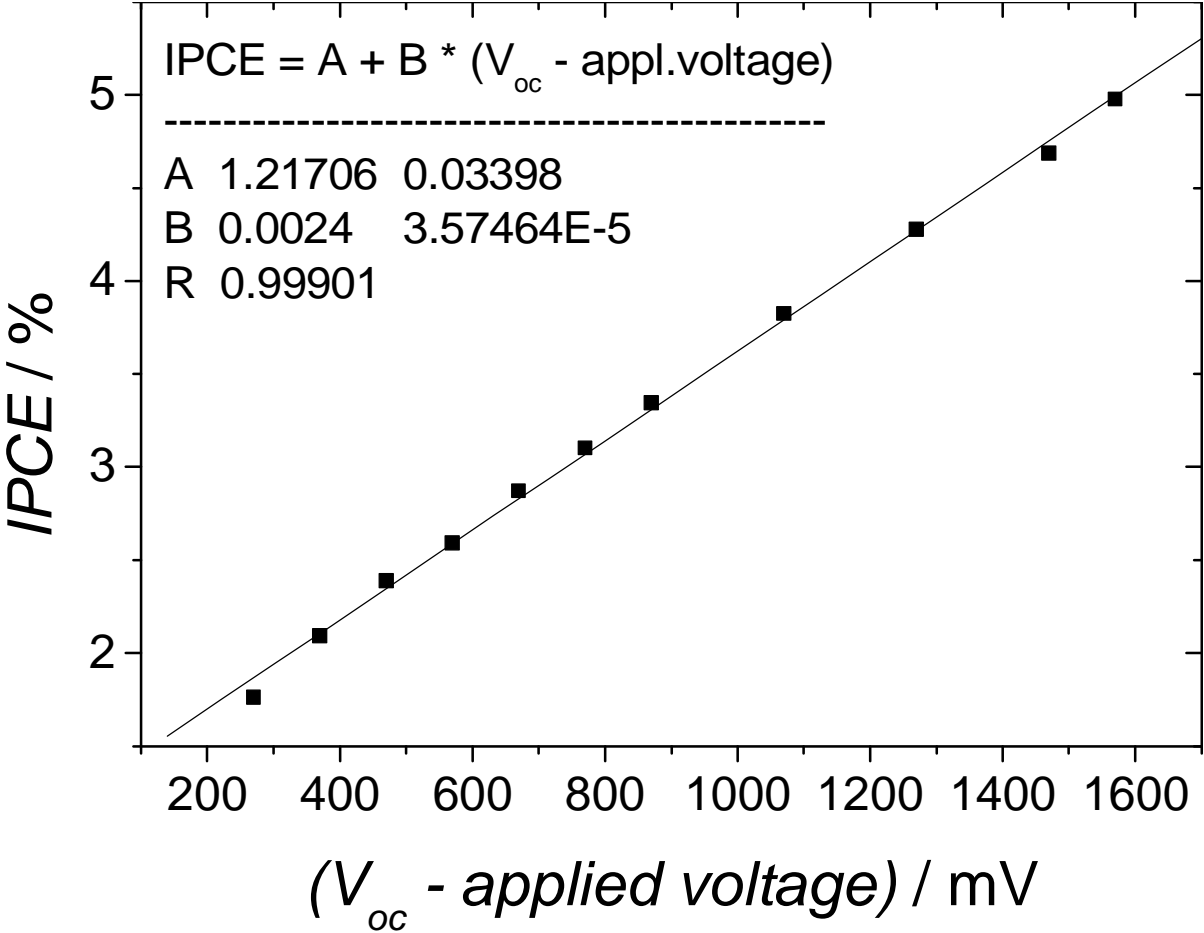
Figure 39: Linear fit of the voltage dependent *IPCE* @ 576 nm of an glass / PEDOT:PSS / 75 nm ZnPc / 25 nm C_{60} / LiF / Al device. The insert shows the fit parameter.

Another observed phenomenon is that the *IPCE* starts to increase stronger at a certain voltage, as Figure 40 shows. The diode is breaking down under illumination. Therefore in this case the Gärtner model can only be investigated for voltages between (+) V_{oc} and − 1000 mV.

The insert text reads:

IPCE = a + b * (appl. voltage)^c
Chi^2/DoF = 0.00017
R^2   = 0.93313

a 1.83318   ±0.03031
b 0.00895   ±0.0012
c 0.5   ±0

x-axis: $(V_{oc} - applied\ voltage)$ / mV

y-axis: *IPCE* / %
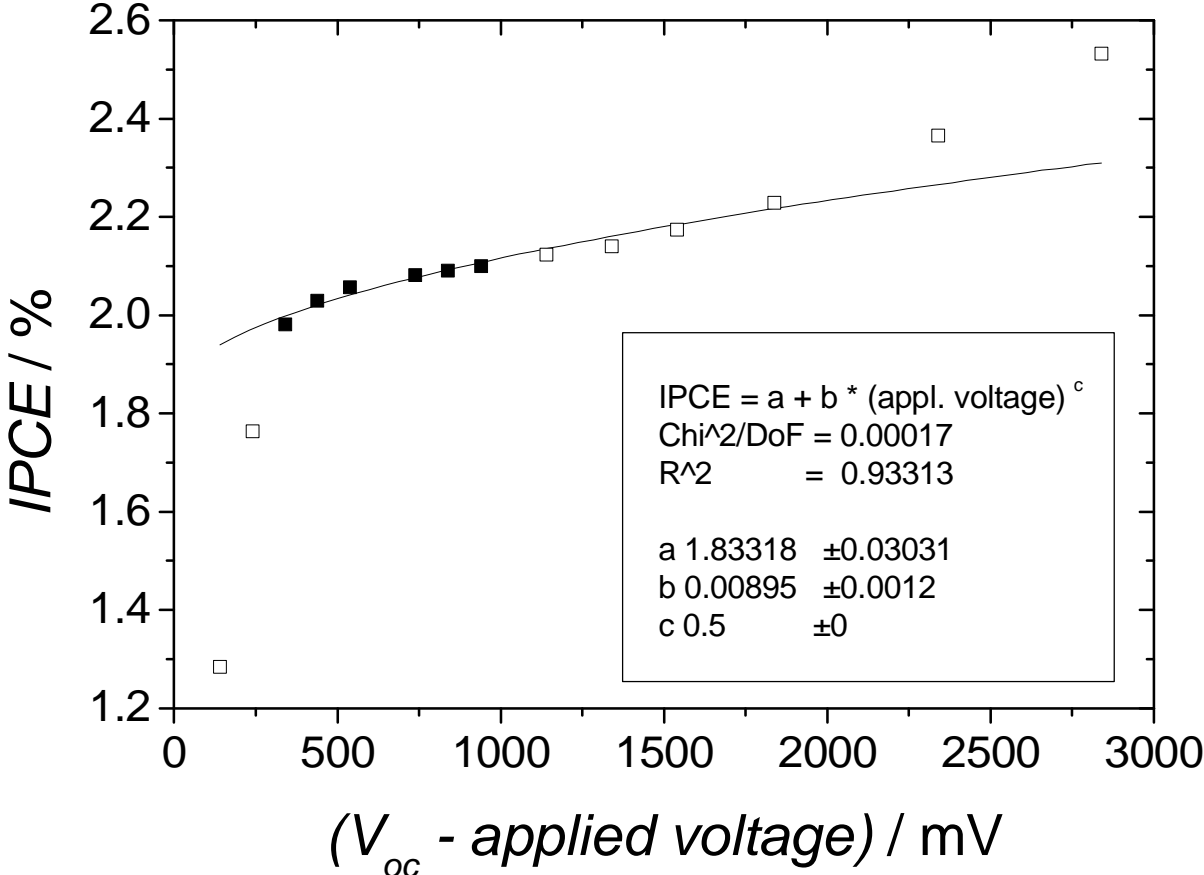
Figure 40: Square root fit of the voltage dependent *IPCE* @ 576 nm of an glass / PEDOT:PSS / about 60 nm ZnPc / about 70 nm C_{60} / LiF / Al device. The insert shows the fit parameters. Note: Only the filled squares were used for the fit.

Normalizing the voltage dependent *IPCE* spectra shows that the increase of the signal with applied negative voltage is stronger at wavelengths where C_{60} is absorbing. The square root fit (Figure 38) is valid for all peaks, but the parameters a and b are different for each peak.

Figure 41: Normalized *IPCE* spectra with applied voltage of the following device: glass / ITO / PEDOT / about 60 nm ZnPc / about 70 nm C_{60} / LiF / Al

5 CONCLUSION

In the Gärtner model the photocurrent is proportional to the thickness of the space-charge-region, which is proportional to the square root of the applied voltage.

This model is investigated for organic bilayer devices using ZnPc and C_{60} as active materials. The investigation is done by voltage dependent *IPCE* measurements: A peak of the *IPCE* spectrum is chosen and for this wavelength the *IPCE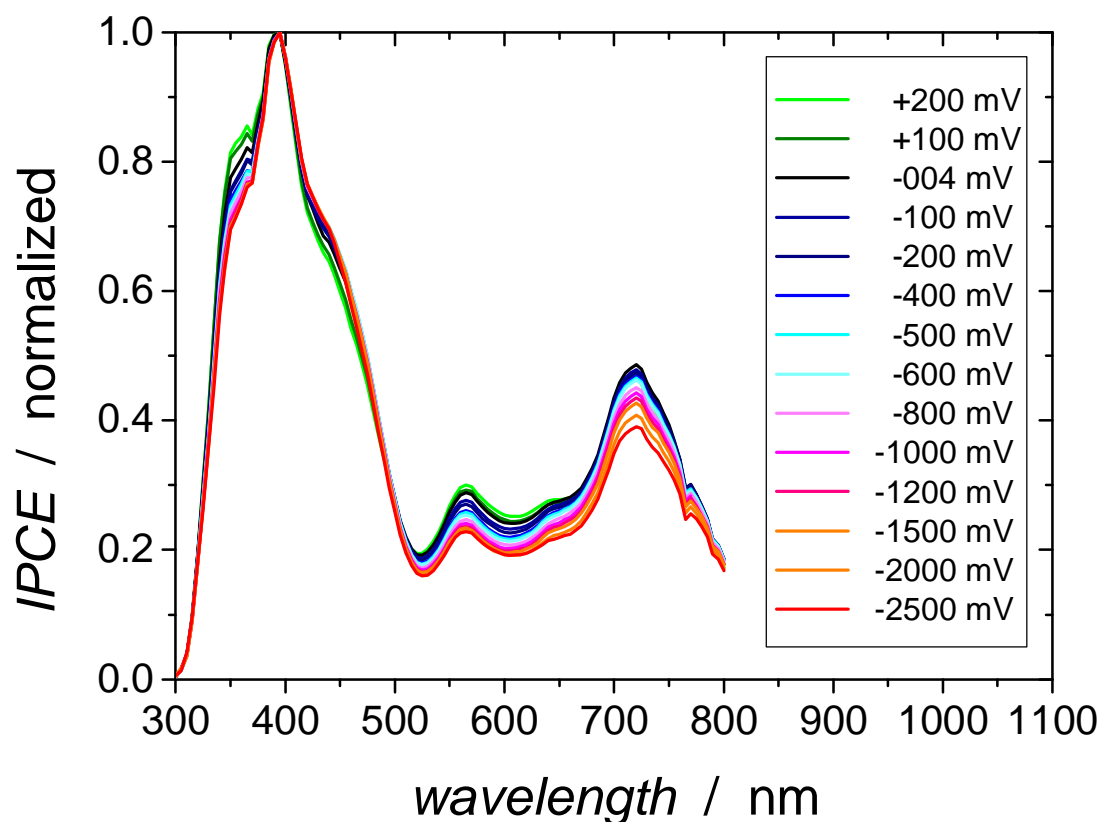* intensity is plotted versus the applied voltage. These plots show square root dependent behaviour, which is predicted by the Gärtner model. Values next to V_{oc} have to be excluded from the fit because of strong photoconductivity effects. Also values that are further than 1000 mV away from V_{oc} have not been taken into account because many diodes start to break down at these bias voltages.

Taking these restrictions into account the Gärtner model is valid for ZnPc / C_{60} bilayer solar cells under illumination, if the films are thick enough to be continuous. This supports the existence of a space charge region at the illuminated interface.

6 REFERENCES

[1]   J. Leggett, *PHOTON International*, Dezember 2004, 80

[2]   A. Jäger-Waldau „Status Report 2004: Energy End-Use Efficiency and Electricity from Biomass, Wind and Photovoltaics in The European Union", EUR 21297 EN

[3]   M. Scharber, A. Hinsch, K. Fostiropoulos, *„Photovoltaik – Neue Horizonte: Jahrestagung des ForschungsVerbunds Sonnenenergie 2003"*, Berlin, 111-115

[4]   http://www.photon.de/news/2004-01%2019%20F&T%20kub%20Po lymerzelle%20von%20Siemens.htm (19.12.2004)

[5]   C.W. Tang, *Appl. Phys. Lett.*, **48**, 1986, 183-185

[6]   J. Rostalski, Dissertation: *"Der photovoltaisch aktive Bereich molekularer organischer Solarzellen"*, RWTH Aachen, 1999

[7]   S. Siebentritt, Dissertation: *„Untersuchung der Mechanismen von Ladungsträgererzeugung und Ladungsträgertransport in ZnPc-Dünnfilmen"*, Universität Hannover

[8]   S. Günster, Dissertation: *„Herstellung und Untersuchung von ‚p/n'-Heterosolarzellen aus den organischen Farbstoffen Phthalocyanin und Perylen"*, Universität Oldenburg

[9]   dimethyl-perylene-tetracarboxylic-diimide

[10]   J. Xue, S. Uchida, B.P. Rand, S.R. Forrest, *Appl. Phys. Lett.*, **85**, 2004, 5757-5759

[11]   H. Hoppe, N.S. Sariciftci, *J. Mater. Res.*, **19**, 2004, 1924-1945

[12]   P. Peumans, A. Yakimov, S.R. Forrest, *J. Appl. Phys.*, 93, 2003, 3693-3723

[13] bathocuproine

[14] S. Heutz, P. Sullivan, B.M. Sanderson, S.M. Schultes, T.S. Jones, *Sol. Energy Mat. & Sol. Cells*, **83**, 2004, 229-245

[15] 4,4′,4″-tris(3-methylphenylphenylamino)triphenylamine (m-MTDATA) p-doped with tetrafluoro-tetracyano-quinodimethane (F4-TCNQ)

[16] dimethyl-perylene-tetracarboxylic-diimide (MPP) n-doped with „Rhodamine B"

[17] D. Gebeyehu, B. Maennig, J. Drechsel, K. Leo, M. Pfeiffer, *Sol. Energy Mat. & Sol. Cells*, **79**, 2003, 81-92

[18] P. Peumans, S.R. Forrest, *Appl. Phys. Lett.*, **79**, 2001, 126-128

[19] T. Haueisen, Diplomarbeit: *„Untersuchung von Gaseinflüssen auf organische Solarzellen"*, Universität-Gesamthochschule-Siegen

[20] M. Martin, J.-J. André, J. Simon, *J. Appl. Phys.*, **54**, 1983, 2792-2794

[21] P. Day, M.G. Price, *J. Chem. Soc. A*, 1969, 236

[22] S. Günster, S. Siebentritt, D. Meissner, *Mol. Cryst Liq. Cryst.*, **229**, 1993, 111-116

[23] J. Rostalski, D. Meissner, *Sol. Energy Mat. & Sol. Cells*, **63**, 2000, 37-47

[24] H. Mizuseki, N. Igarashi, R.V. Belosludov, A.A. Farajian, Y. Kawazoe, *Synthetic Met.*, **138**, 2003, 281-283

[25] H. Neugebauer, M.A. Loi, C. Winder, N.S. Sariciftci, G. Cerullo, A. Gouloumis, P. Vázquez, T. Torres, *Sol. Energy Mat. & Sol. Cells*, **83**, 2004, 201-209

[26] M.A. Loi, P. Denk, H. Hoppe, H. Neugebauer, C. Winder, D. Meissner, C. Brabec, N.S. Sariciftci, A. Gouloumis, P. Vázquez, T. Torres, *J. Mater. Chem.*, **13**, 2003, 700-704

[27] T.M. Brown, J.S. Kim, R.H. Friend, F. Cacialli, R. Daik, W.J. Feast, *Appl. Phys. Lett.*, **75**, 1999 ,1679-1681

[28] J.S. Kim, M. Granström, R.H. Friend, N. Johansson, W.R. Salaneck, R. Daik, W.J. Feast, F. Cacialli, *J. Appl. Phys.*, **84**, 1998, 6859-8870

[29] Y. Park, V. Choong, Y. Gao, B.R. Hsieh, C.W. Tang, *Appl. Phys. Lett.*, **68**, 1996, 2699-2701

[30] H.B. Michaelson, *J. Appl. Phys.*, **48**, 1977, 4729-4733

[31] T. Oekermann, D. Schlettwein, D. Wöhrel, *J. Appl. Electrochem.*, **27**, 1997, 1172-1178

[32] R.W. Lof, M.A. van Veenendaal, B. Koopmans, H.T. Jonkman, G.A. Sawatzky, *Phys. Rev. Lett.*, **68**, 1992, 3924-3927

[33] P. Peumans, S.R. Forrest, *Appl. Phys. Lett.*, **79**, 2001, 126-128

[34] R. H. Bube, *"Photoelectronic Properties of Semiconductors"*, Cambridge University Press, 1992

[35] H. Ibach, H. Lüth, *"Festkörperphysik"*, Springer-Verlag Berlin Heidelberg, 1990

[36] S. M. Sze, *"Physics of Semiconductor Devices"*, John Wiley & Sons, Inc. New York, 1981

[37] H.-J. Lewerenz, H. Jungblut, „*Photovoltaik – Grundlagen und Anwendungen*", Springer-Verlag, 1995, 71

[38] L.A.A. Pettersson, L.S. Roman, O. Inganäs, *J. Appl. Phys.*, **86**, 1999, 487-496

[39] H.W. Kroto, J.R. Heath, S.C. O'Brien, R.F. Curl, R.E. Smalley, *Nature*, **318**, 1985, 162-163

[40] T.M. Brown, R.H. Friend, I.S. Millard, D.J. Lacey, T. Butler, J.H. Burroughes, F. Cacialli, *J. Appl. Phys.*, **93**, 2003, 6159-6172

[41] C.J. Brabec, S.E. Shaheen, C. Winder, N.S. Sariciftci, P. Denk, *Appl. Phys. Lett.*, **80**, 2002, 1288-1290

[42] C. Winder, Dissertation: *„To Increase the Photon Harvesting in the Photoactive Layer of Bulk Heterojunction Organic Solar Cells"*, JK University Linz, 2004, page 3-2

[43] B. Kessler, *Appl. Phys. A*, **67**, 1998, 125-133

[44] M. Murgia, F. Biscarini, M. Cavallini, C. Taliani, G. Ruani, *Synthetic Met.*, **121**, 2001, 1533-1534

[45] H. Hoppe, N. Arnold, D. Meissner, N. S. Sariciftci, *Thin Solid Films*, **451-452**, 2004, 589-592

[46] H. Hoppe, N. Arnold, D. Meissner, N. S. Sariciftci, *Sol. Energy Mat. & Sol. Cells*, **80**, 2003, 105-113

CURRICULUM VITAE

Name:	Martin Egginger
Date of Birth:	29th October 1977
Birthplace:	Salzburg
Nationality:	Austrian
Marital Status:	Unmarried
Children:	Laura, 5th March 2004
Parents:	Peter Egginger, pharmaceutical representative for Pfizer Inc
	Renate Egginger, primary school teacher

Education:

09 / 2003 – 12 / 2004:	Diploma Thesis at the *institute for physical chemistry*
10 / 1997 – 02 / 2005:	Studies at the university of Linz:
	economical engineering of technical chemistry
06 / 1996:	School leaving exam passed with distinction
1988-1996:	Grammar school in Salzburg
1984-1988:	Primary school in Grödig

Military Service:

10 / 1996 - 05 / 1997	Supply unit Salzburg / Schwarzenbergkaserne

Languages:

since 1987:	English in word and language
since 1992:	French in word and language
1990-1996:	Latin

Related Experience:

09 / 2003:	Summerschool "Basic principles and new concepts in quantum solar energy conversion", Hirschegg, Austria
08 / 2003 – 09 / 2004:	project collaborator at the *institute for physical chemistry*
07 – 09 / 2002:	project collaborator at the *institute for physical chemistry*
03 – 06 / 2002:	Tutor at the *institute of inorganic chemistry*

10 / 2001 – 01 / 2002:	Tutor at the *institute of inorganic chemistry*
	(www.jku.at/a2c)
Summer 2000, 2001:	Electro-chemical process optimization at
	Sony DADC Austria PLC (www.sonydadc.com)

Further Employers:

Summer 1998, 1999:	CD - production at *Sony DADC Austria PLC*
Summer 1996, 1997:	*Leiner Salzburg* (www.leiner.at)
Summer 1994, 1995, 1996:	*Pressegroßvertrieb Salzburg* (www.pgvsalzburg.com)

Additional Experience:

01 / 2002 – 08 / 2004:	Financial manager of *AIKIKAI – VöA* (www.aikikai.at)
10 / 2002 – 09 / 2003:	Head of *ESH* representation (www.esh.uni-linz.ac.at)
05 / 2003:	Chief Organizer of "Heimfest des *ESH*"
	(event with 3500 visitors)
03 / 2003:	Chief Organizer of "Frühlingsball des *ESH*"
	(event with 500 visitors)
10 / 2001 – 09 / 2002:	Financial manager of *ESH* representation
01 – 06 / 2002:	Children's teacher at *AIKIKAI – VöA*
10 / 2001 – 01 / 2002:	Dancing teacher at *ESH Linz*
1995 – 2000:	Auditor of the *dance-sports-club Team7*
11 / 1995:	Organizer of Ball des Akademischen Gymnasiums
	(event with 1500 visitors)

Additional Qualifications:

Driver's license since 1995; Yacht Masters Licence

Hobbies:

AIKIDO, sailing, snowboarding, dancing, travelling

Contributions to conferences:

Poster:	"Investigating the Space Charge Region in Organic Solar Cells"
	M. Egginger, D. Meissner, S. N. Sariciftci
	EUROPV 2004, Kranjska Gora, Slovenia

EIDESSTATTLICHE ERKLÄRUNG

Ich erkläre an Eides statt, dass ich die vorliegende Diplomarbeit selbstständig und ohne fremde Hilfe verfasst, andere als die angegebenen Quellen und Hilfsmittel nicht benutzt bzw. die wörtlich oder sinngemäß entnommenen Stellen als solche kenntlich gemacht habe.

Linz, den _____   _____

(Martin Egginger)